Title:

Hypothalamus-specific NSCs derived from hPSCs ameliorate age-associated dysfunction upon transplantation into aged mouse hypothalamus

Yanuar Alan Sulistio[2,§] , Yuna Lee[4,5,§], Kelvin Pieknell[2,§], Sebin Hong[2-3], Jumi Kim[2-3], Min Jong Seok[2-3,] Na-Kyung Lee[2-3], Kyu-Sang Park[6], Taeui Hong[6], Suyeon Choi[6], Ki Woo Kim[7], Dong Joo Yang[7], Woong-Yang Park[8,9], Kyung Yeon Han[8,9], Seul Gi Yoon[10], Il Yong Kim[10,11], Je Kyung Seong[10,11], Tae Yong Lee[12,13], Min Sung Kim[12,13], Min Soo Kim[4,5,*], Sang-Hun Lee[1-3,*]

[1]Department of Biochemistry and Molecular Biology, College of Medicine, Hanyang University; Seoul, South Korea

[2]Hanyang Biomedical Research Institute, Hanyang University; Seoul, South Korea

[3]Graduate School of Biomedical Science and Engineering, Hanyang University; Seoul, South Korea

[4]Brain Science Institute, Korea Institute of Science and Technology (KIST); Seoul, South Korea

[5]Division of Bio-Medical Science and Technology, KIST School, University of Science and Technology; Seoul, South Korea

[6]Mitohormesis Research Center, Yonsei University Wonju College of Medicine; Wonju, South Korea

[7] Division of Physiology, Departments of Oral Biology and Applied Life Science, BK21 FOUR, Yonsei University College of Dentistry; Seoul, Korea

[8]Geninus Inc.; Seoul, South Korea

[9]Samsung Genome Institute, Samsung Medical Center; Seoul, South Korea

[10]Korea Mouse Phenotyping Center (KMPC), Seoul National University; Seoul, South Korea

[11]Laboratory of Developmental Biology and Genomics, Research Institute for Veterinary Science, and BK21 PLUS Program for Creative Veterinary Science Research, College of Veterinary Medicine, Seoul National University; Seoul, South Korea

[12]Central Research Center, Corestem Inc; Seoul, South Korea

[13]College of Pharmacy, Chungbuk National University; Cheongju, South Korea

[§]These authors contributed equally.

*Correspondence: Sang-Hun Lee, M.D., Ph.D., Department of Biochemistry and Molecular Biology, College of Medicine, Hanyang University, Seoul, 04763, South Korea. Telephone: 82-2-2220-0625; Fax: 82-2-2220-2422; E-mail: leesh@hanyang.ac.kr; or Min Soo Kim, Ph.D., Brain Science Institute, Korea Institute of Science and Technology (KIST), Seoul, 02792, South Korea. E-mail: minsoo.kim@kist.re.kr.

One Sentence Summary

hPSC-derived hypothalamus NSCs mitigate age-associated physiological decline upon transplantation into the hypothalamus of aged mice.

Abstract

The hypothalamus is the brain region that regulates systemic body metabolism and multiple functions in other brain regions. In adult mice, the hypothalamus harbors neural stem/precursor cell (NSC)-like cells. Along with the dysregulation of body metabolism and physiology that occurs during aging, the NSC population in the hypothalamus declines with age. Here, we introduce a novel protocol that yields scalable and storable hypothalamus-specific NSCs (htNSCs) from human pluripotent stem cells (hPSCs). Implanting htNSCs into the medio-basal hypothalami of aged mice conspicuously ameliorated age-related declines in metabolic fitness, physical capacity, and cognitive function and produced corresponding histologic changes in various body tissues. Single transcriptome and immunohistochemical analyses of the grafted hypothalamic tissues showed that the anti-aging effects were attained by correcting glial NF-κB, TNF-α, and NLRP3 inflammasome pathways. Collectively, our findings support the potential of anti- or healthy aging therapies that target htNSCs and hypothalamic inflammation.

Keywords: Hypothalamus; Hypothalamic neural stem cells; Human pluripotent stem cells; Aging; Anti-aging; Metabolism; Inflammation; Inflammaging; NF-κB; Microglia

INTRODUCTION

The hypothalamus is a small brain region that plays a critical role as a master regulator of the body's systemic metabolism and homeostasis by sensing and integrating responses to peripheral environmental and nutritional cues. In addition, the hypothalamus has neurocircuitry connections with other brain regions that regulate brain physiology, including hippocampal memory and cognitive functions (1-6). The body and brain functions regulated by the hypothalamus gradually deteriorate during aging. Thus, it is proposed that cellular mechanisms operating in the hypothalamus are possible targets in the development of anti-aging and aging-control technologies (7).

Hypothalamic functions are governed by intricate neuro-circuitry networks involving a myriad of neuronal subtypes with hypothalamus-specific neuro-endocrine and neuro-transmission functions. In addition, growing evidence indicates that non-neuronal glial cells play equally important roles in the hypothalamus, such orchestrating intra-hypothalamic functions and the hypothalamic response to metabolic cues from the body, by participating in synaptic transmission, synaptic plasticity, and nutrient/hormone sensing (8-12). Given that aging and neurodegenerative diseases cause more drastic changes in the transcriptomes and phenotypes of glia than of neuronal cells (13-19), researchers have begun to focus on glial cells. Furthermore, in the adult brain, specifically within the third-ventricle wall and median eminence, the hypothalamus harbors distinct cells known as tanycytes, which possess neural stem cell properties (20, 21). Tanycytes in the hypothalamus are multifunctional, playing key roles in physiological regulation. They convey metabolic status to hypothalamic neurons, moderate orexigenic/anorexigenic neuronal activity, and manage the hormonal output of the hypothalamic-pituitary-thyroid axis (22-24). Recent research reveals part of tanycytes act as quiescent neural stem cells in the adult brain, capable of generating new hypothalamic neurons, underscoring their importance in neural regulation and regeneration (25, 26) (Hereafter, 'tanycyte' will refer to the quiescent hypothalamus NSCs in the adult hypothalamus, while 'hypothalamus NSC' (htNSC) will be used as a general term, regardless of developmental and proliferation stages).(22-27) Of note, these htNSCs gradually diminish with age and are almost entirely lost in advanced aging

(8). They further showed that aging processes were retarded in old mice that were transplanted with hypothalamus-specific NSCs derived from postnatal mouse brains, suggesting htNSC replacement as an anti-aging strategy (8).

Despite the great clinical importance of the hypothalamus, studies on hypothalamic functions have been made exclusively in animal models. Their translation to humans remains nascent, mainly due to the inaccessibility of human hypothalamic tissues and cells. Several studies have generated hypothalamic neuronal cell types from human pluripotent stem cells (hPSCs) (28-30). Given the functional significance of glia and htNSCs in the hypothalamus, however, it is compelling to develop research platforms that can provide diverse hypothalamic cell types, including non-neuronal cells, of human origin. To this end, we have developed a method for differentiating hPSCs into htNSCs with neuro- and gliogenic potential by adopting hypothalamus region–specific patterning in hPSC-derived brain organoids (31), followed by NSC preparation from early hypothalamus-like brain organoids. With a clinical translation of the htNSC-based anti-aging strategy in mind, we implanted our hPSC-derived human htNSCs into the hypothalami of aged mice and analyzed the systemic anti-aging effects in those animals.

RESULTS

Generation of htNSCs from hPSC-derived hypothalamus-like organoids

Preparing brain region–specific NSC cultures from differentiating hPSCs was frequently infeasible due to cell apoptosis/senescence and the loss of regional identity among the patterned cells during the procedure for cell dissociation and replating, which is required to isolate an NSC population from differentiating hPSCs (32, 33). In our previous study (33), we improved the problem of NSC preparation by inducing neural induction/patterning in a 3D organoid culture environment, whereby we successfully prepared midbrain-specific NSCs for use in Parkinson’s disease therapy. In this work, we leveraged the principles and advantages of the organoid-based method to prepare human htNSCs from hPSCs. To this end, human embryonic stem cells (hESC, H9) were induced to differentiate into hypothalamus-like organoids in the presence of small molecules for inducing hypothalamic fate (28-30) (Fig. 1A and Suppl. Fig.

S1A-B). The combinations, concentrations, and treatment periods of the hypothalamic patterning molecules were optimized based on high expression of the hypothalamus–specific markers *RAX*, *NKX2-1*, *OTP*, *ILS1*, and *SF-1* and low expression of the midbrain marker Engrailed-1 (*EN1)* (Suppl. Fig. S1A). Treatment with SHH and purmorphamine during early organoid differentiation was indispensable for hypothalamus-specific marker expression (Fig. 1B and Suppl. Fig. S1A). Further addition of CHIR, CNTF, IWP-2, XAV, and FGF8, which have been reported as molecules for hypothalamic patterning (28-30), did not enhance but lower hypothalamic marker expression (Suppl. Fig. S1A). Cells dissociated from the organoids on DIV 20 were efficiently sub-cultured as monolayer. Generated htNSCs expressed markers specific for general NSCs (SOX2, NESTIN), proliferating cells (KI67), and hypothalamic specific markers, indicating efficient generation of a homogenous htNSC culture from the early stage of the organoids (Fig. 1B–C). The expressions of hypothalamus-specific markers and the percentage of Nestin+ and RAX+ htNSCs in our method were significantly higher compared to those observed in htNSC cultures generated using other published protocols (28, 29) (Suppl. Fig. S1B-E). To further confirm their hypothalamic identity, we performed RNA sequencing (RNA-seq) on our cultured htNSCs. When comparing our htNSC transcriptome profile to various adult human brain transcriptome (GTEx Database, ages of 22-68 years), the htNSC was clustered together with the human adult hypothalamus, signifying a high hypothalamic regional identity (Fig. 1D).

Additionally, the htNSCs were expandable for extended periods (Fig. 1E), could be stored and re-cultured from liquid N2 without loss of viability or naïve htNSC-specific marker expression (Fig. 1F), establishing the htNSC culture derived from hPSC-organoids as a stable and readily available source of human htNSCs. Proliferation, indicated by PDL and Ki67 protein levels, decreased at late passages (Fig. 1E and Suppl. Fig. S2A), signifying replicative senescence. Y-box protein 1 (YB-1) has been reported recently to be expressed in htNSCs of young mouse hypothalamus and its level declines during aging via its protein degradation (34). Consistent with previous results, YB-1 was also highly expressed in the human htNSC cultures. However, the protein level showed a decline in late cell passages, despite no alteration in mRNA expression, accompanied by a reduction of the cell proliferation marker Ki67 expression (Suppl. Fig. S2A–B). These outcomes suggest a shared role of YB-1 in preventing replicative

senescence in htNSCs across the species.

Differentiation phenotypes of the hPSC-derived htNSCs

Upon terminal differentiation, the htNSCs could differentiate into mature neurons expressing (TUBB3, MAP2, RBFOX3 (NeuN), and synapsin-1). It also expressed hypothalamus-specific neuropeptides such as POMC, NPY, SCGN, and PMCH (Fig. 1G). Astroglial cell population was detected in the differentiated htNSC cultures (Fig. 1G), which increase in proportion in the later passages (Fig. 1H). Hypothalamic neurons and astrocytes sense the nutritional status of the body through peptides such as leptin and ghrelin that are generated in peripheral organs. An administration of leptin to the differentiated htNSC cultures activated the major leptin-mediated STAT intracellular pathway, which was shown by increased phosphorylated STAT3 (pSTAT3) levels in Western-blot analysis (Fig. 1I, left). In addition, the activation of FOXO1, the intracellular signal transducer of ghrelin, occurred when the differentiated htNSC cultures were treated with ghrelin (Fig. 1I, right), indicating that the differentiated hypothalamic cells functionally sensed nutritional cues. Using this protocol, htNSCs with neurogenic and gliogenic capacities were also generated from the human induced pluripotent stem cell (hiPSC) lines CMC-hiPSC-011 and CS-001(Suppl. Fig. S3).

Next, we performed a single-cell RNA-seq (scRNA-seq) analysis of the differentiated htNSC culture at terminal differentiation, day 70. After filtering doublets and clusters cells with low-quality reads, we used 6,394 cells for the analysis. Unsupervised clustering of the dataset revealed thirteen clusters, which were projected onto a uniform manifold approximation (UMAP) map for visualization. On the basis of the expression levels of well-characterized marker genes (35-37) alongside with automated identification using scType, the cluster identities were designated as proliferating neural stem cells (NSCs), intermediate progenitor cells (Int1, 2), interneuron progenitor cells (iNPCs), astrocyte progenitor cells (APCs), neurons (Neu1, 2), astrocytes (Ast1, 2, 3), radial glia (RGs), proteoglycan-secreting glia (PGGs), and tanycytes (Tan) (Fig. 2A-C and Suppl. Fig. 4A). For unbiased confirmation of the hypothalamic fate, we mapped the gene expression signatures of the cell clusters to the mouse brain transcriptome (at post-natal day 28) in the Allen Developing Brain Atlas using Voxhunt (38). Significantly, our

scRNA-seq profiles showed that every identified cluster in the differentiated htNSC culture precisely corresponded to the hypothalamic region of the atlas (Fig. 2D and Suppl. Fig. S4B). Furthermore, the progenitor and intermediate cell clusters (Int1, Int2, iNPC, APC, NSC) were enriched to the hypothalamic region adjacent to the ventricular area, where adult neurogenesis occurs (Fig. 2D and Suppl. Fig. S4B). To provide additional confirmation, we cross-referenced our single-cell transcriptome data with published datasets of human fetal hypothalamus (gestational week (GW) 18-22) (Suppl. Fig. S4C-D) (39). The clustering analysis indicates that our single-cell transcriptome data align closely with the human fetal hypothalamus datasets (Suppl. Fig. S4E-F). Expectedly, oligodendrocytes and microglia were absent in the differentiated htNSC (Suppl. Fig. S4G). Next, we performed a gene regulatory network analysis using pySCENIC and identified the potential upstream master regulator (regulon) of each cell cluster (Suppl. Fig. S4H).

The hypothalamus is a complex brain area that contains myriad subtypes of neurons with neuroendocrine and neurotransmitter identities. To unravel the identity of the neuronal populations in our differentiated htNSC cultures, we performed further clustering on the neuronal clusters (Neu1 and Neu2). Upon re-clustering based on the signature transcripts, we detected 8 subclusters of neurons (n1–n8) (Fig. 2E), comprising neuronal clusters with different neurotransmitter identities, such as glutamatergic (n6), GABAergic (n2), dopaminergic (n8), and dopaminergic/glutamatergic (n1, n3, n4), and clusters with specific hypothalamic neuroendocrine identities, such as those expressing *SCGN* (n5), *PMCH* (n4), *TRH* (n3), and *NR3C1* (n1) (Fig. 2F and G). Sleepwalk analysis to validate that the clusters represented in the UMAP space are grouped properly according to their Euclidean distance (Suppl. Fig. S4I). In addition, the neuronal subclusters were classified by their unique transcriptional factors and regulons (Fig. 2F and G). Of note, *VGF*, a gene that is highly enriched in the adult hypothalamic neurons (40, 41), was widely expressed throughout the neuronal clusters (Fig. 2F).

The APC cluster branched into three astrocyte trajectories (Fig. 2H). Astrocytes share a region-specific gene transcription profile in parallel with its neuronal counterpart (42, 43), and the region-specific roles of astrocytes are well acknowledged. Consistently, a hypothalamus-specific

transcriptome signature (*CRYM, SCG2, RAX, FGF10, COL25A1, GPC3, DIO2*) was identified in the astrocytic clusters of the differentiated htNSC culture (Fig. 2I). MANF, significantly present in the adult hypothalamus and a key player in hypothalamic control of food intake and energy balance, was prevalent in all astrocytic cell lineage clusters but predominantly in the APC cluster (Fig. 2I and Suppl. Fig. S5E). This aligns with its highest expression in the early postnatal brain (44),(45). Astrocyte cluster Ast2 is regarded as a homeostatic astrocytic population that expresses *SLC1A3* (GLAST) and provides metabolic support for neighboring neurons (Fig. 2I). Additionally, Ast2 could be involved in neuroendocrine functions because of its specific expression of genes such as *SLCO1C1* (thyroid hormone transporter), *CRYM* (Crystalin Mu, a thyroid hormone binding protein), and *SCG2* (secretogranin II, a neuroendocrine secretory protein) (Fig. 2I). By contrast, Ast1 preferably expressed genes related to immune function such as *RSAD2* and *TRIL* (Fig. 2I). Moreover, interferon-induced genes, such as *ISG5*, *IFIT*, and *STAT1*, were also specifically expressed in Ast1, suggesting a reactive phenotype. Aside from the "classical" homeostatic and reactive astrocytes, we also detected a third type of astrocyte (Ast3) that was derived from common progenitor cells (APCs) and expressed astrocyte-related transcription factors (*SOX9*, *ID3*, *BHLHE41*) and common astrocyte markers (*APOE*, *AQP4*, *SPARCL1*, *SPARC*) but was devoid of *GFAP* (Fig. 2I). Ast3 is characterized by gene expression specific for not only tight junction formation (*CLDN5*, *ALCAM*, *COL1A2*), but also the astrocyte population in the adult subventricular zone (*Meis2*, *Col1a2*), which interacts with ependymal cells or pericytes (46-48). Of note, a cluster was designated as a tanycyte-like population because it exclusively expressed tanycyte-specific markers such as *RAX*, *FGF10*, *COL25A1*, *GPC3*, and *DIO2* (Fig. 2I). Interestingly, *LEPR* (leptin receptor) expression was detected in the tanycyte cluster (Fig. 2I), supporting the involvement of tanycytes in metabolic homeostasis via leptin signaling (22).

***In vitro* htNSC differentiation recapitulated hypothalamic brain development**

Next, we used Monocle 3 to perform pseudo-temporal ordering of the transcriptional dynamics of the cell clusters that were differentiated from human htNSCs. Consistent with brain development, in which neurons and astrocytes arise sequentially from common progenitors, the UMAP clustering shows that the intermediate progenitor cell clusters (Int1, 2) were bifurcated

into neurons (Neu1, 2) and the APC cluster that gave rise to the astrocytic populations (Ast1–3) (Suppl. Fig. S5A). Several genes showed temporal dynamic changes in gene expression that recapitulated those in the developing brain. For example, a steep decrease in the expression of the proliferation marker *CDK1* at an early time point was followed by a surge in the expression of the pro-neural gene *ASCL1* at the late progenitor cell stage and increased expression of the neuron-specific *TUBB3* and *SNAP25* at the terminal stage of the neuronal trajectory (Suppl. Fig. S5B). The *SLIT-ROBO* signal has recently been identified as a critical regulator of hypothalamus-specific brain development (49). Of note, the *SLIT-ROBO* signal genes in the differentiated htNSC cultures showed pseudo-time patterns similar to those of *in vivo* hypothalamic brain development (Suppl. Fig. S5C), indicating our *in vitro* htNSC differentiation recapitulates hypothalamus development *in vivo*.

Thus far, the developmental origin of tanycytes has been unidentified. Interestingly, consistent with a developmental trajectory analysis suggesting that tanycytes originate from the astrocyte population during hypothalamic brain development (49), our pseudo-time analysis indicates that tanycyte-like cells (Tan) developed from the early Ast2 population (Suppl. Fig. S5D and E).

Age-associated declines in physical and cognitive activity were ameliorated in mice that received hPSC-derived htNSCs

Physical strength, muscle endurance, motor coordination, memory, and cognitive function are all declining with age (14), and those age-associated changes are linked to hypothalamic dysfunction in regulating body metabolism and homeostasis (50). A previous study has shown that age-associated impairment of physical and cognitive activity could be delayed by implantation of htNSCs derived from mouse pups (8). To take a critical step toward the clinical translation of the htNSC-based anti-aging strategy, we transplanted single dissociates of human htNSCs (passage 2-3) prepared from the hESC (H9)-derived hypothalamus-like organoids into the hypothalami of mice at 12-months of age (Fig. 3A). The mouse htNSCs derived from newborn mice, which were used in the previous study (8), survived poorly after implantation into the mouse hypothalamic region, and thus genetic engineering with dominant recombinant IκB to inhibit the NF-κB inflammatory signal was needed to overcome the survival problem (8). By

contrast, upon transplantation into the medio-basal hypothalamus (MBH), the hPSC-derived human htNSCs survived and integrated efficiently into the host hypothalamus, forming human-specific marker (hNCAM or human mitochondrial-specific antigen)-positive grafts, portions of which expressed undifferentiated htNSC (RAX), differentiated neuronal (NeuN), and astrocytic (human GFAP, hGFAP) markers 2–4 weeks post-transplantation (Fig. 3B–C).

To ensure reproducibility, we designed multiple rounds of cell transplantation with independently prepared human htNSCs and aged mice. In those consecutive trials of htNSC transplantation, the mice that received transplantation displayed a significant improvement in exploratory behavior and locomotor activity (Fig. 3D), coordination (rotarod) (Fig. 3E), muscle endurance (grip) (Fig. 3F), and treadmill performance (Fig. 3G), compared with the age-matched sham-operated control mice (control, N2 medium-injected). Furthermore, the long-term and spatial memory and cognitive functions of the grafted mice were significantly improved in the Morris water-maze (MWM; Fig. 3H–I) and novel object recognition tests (Fig. 3J). The physical activities and memory/cognitive functions in the grafted old mice were also compared with the young mice (aged 3-6 months) (Fig. 3 and Suppl. Fig. S6).

Improvement of body energy metabolism and tissue aging by intra-hypothalamic htNSC transplantation

The grafted mice were leaner, devoid of age-dependent body weight gain during the post-transplantation period (12–16 months) that was manifested in the vehicle-injected control mice (Fig. 4A). There was no difference in the food intake and physical activity changes only occurred during the dark cycle (Fig. 4B–C). Consequently, the htNSC grafted mice displayed greater energy expenditure in the metabolic cage compared to control aged mice (Fig. 4D). Body composition analysis indicates that the htNSC-grafted mice had markedly lower fat mass with increased lean mass indicating lower adiposity (Fig. 4E). Accordingly, lipid droplet size was greatly reduced in the inguinal white adipose tissue (iWAT), epididymal white adipose tissue (eWAT), and intrascapular brown adipose tissue (iBAT) of the grafted mice than the control mice (Fig. 4F–H). Similarly, hepatic steatosis in the aged mice was markedly decreased in the transplantation group (Fig. 4I).

Growth/differentiation factor 15 (GDF15) and fibroblast growth factor 21 (FGF21) are key secretory proteins that stimulate peripheral tissues to increase energy expenditure and lipid consumption (51-54). Hepatic GDF15 and FGF21 proteins and their upstream regulator ATF4 were significantly upregulated in the livers of the grafted mice (Fig. 5A). Additionally, FGF21 was also increased in iWAT and eWAT of the grafted mice, which was accompanied by the upregulated protein expression of MT-CO1 and SDHB, mitochondrial proteins that execute energy consumption/thermogenesis (Fig. 5B–C) (55, 56). Consistently, rectal temperature was significantly higher in the htNSC-grafted mice than the controls (Fig. 5D). The hypothalamus controls thermogenesis and energy expenditure by activating the sympathetic nervous system (57). Messenger RNA expression of β1, 2, and 3 adrenoreceptors (*Adrb1*, *Adrb2*, and *Adrb3*) and lipolytic genes (*Dio2* and *Lipe*) was significantly upregulated in the eWAT of the grafted mice (Fig. 5E), collectively implying that aged hypothalami grafted with htNSCs regulated body lipid catabolism/thermogenesis more efficiently than the hypothalami of the control mice by engaging the sympathetic nervous system. Along with efficient energy metabolism, the mice that received intra-hypothalamic htNSC transplantation showed significantly better glucose tolerance than the control mice (Fig. 5F).

In addition to body energy metabolism, the hypothalamus regulates bone remodeling and homeostasis (58). A bone μCT examination showed osteoporotic changes in the tibias and femurs of the control mice at age 16 months (Fig. 5G–H). That bone loss was greatly prevented by intrahypothalamic htNSC transplantation, as evidenced by a significant increase in bone mass density (BMD), bone volume/total volume (BV/TV) ratio, trabecular thickness (Tb.Th.), and trabecular number (Tb.N.) in the grafted mice (Fig. 5G–H). Notably, the increase in bone density coincided with a substantial decrease in the osteoclast population among the transplanted mouse group (Fig. 5I), suggesting that suppression of bone resorption underlies the observed enhancement in bone density. Further interestingly, renal p16 protein expression, which is closely associated with kidney aging (59), was greatly downregulated in the mice that received intra-hypothalamic transplantation (Suppl. Fig. S7).

When we determined cytokine and hormone levels using a cytokine array kit, the blood level of leptin was lower in the grafted mice than in the control mice (Suppl. Fig. S8A–B), which was further validated by ELISA-based quantification (Suppl. Fig. S8C). This is consistent with the positive correlation between the plasma leptin level and body fat mass (60, 61). Furthermore, the lower leptin level reflects the increased bone density observed in the grafted mice (62).

Single-cell transcriptome analysis of aged hypothalamic brains grafted with htNSCs

To identify the transcriptional profile of the grafted hypothalami, we performed a droplet-based single-nucleus RNA-seq (snRNA-seq) analysis of cell nuclei extracted from the transplanted hypothalamus and control groups 4 months post-transplantation. We sampled six hypothalami (three per group) on four independent sequencing runs (two runs per group) (Fig. 6A). After filtering and doublet removal, 12,161 nuclei were clustered and projected onto a two-dimensional UMAP space for visualization (Fig. 6B). We identified 30 clusters: 23 neuron (10 clusters of GABAergic neurons and 13 clusters of glutamatergic neurons), two tanycyte, one astrocyte, one oligodendrocyte, one oligodendrocyte precursor cell (OPC), one microglia, and one pericyte cluster. For the sake of simplicity and general visualization, the 23 neuronal clusters were merged into glutamatergic and GABAergic neuron clusters, as described above, and the two tanycyte clusters were merged into one (Fig. 6B and Suppl. Fig. S9A). The cells were annotated manually based on well-established cellular markers: *Snap25* for pan-neurons, *Gad1* for GABAergic neurons, *Slc17a6* for glutamatergic neurons, *Agt* and *Slc1a3* for astrocytes, *Mbp* and *Plp1* for oligodendrocytes, *Olig2* and *Pdgfra* for OPCs, *P2ry12* and *Cx3cr1* for microglia, *Rax* and *Col23a1* for tanycytes, and *Slc4a7* and *Flt1* for pericytes (Fig. 6C and Suppl. Fig. S9B). Many well-known hypothalamus-specific neuronal subtypes were identified in the neuron subclusters. For example, GABA neuron subcluster 2 (GABA-2), which contained galanin-secreting neurons, are highly enriched in the hypothalamus and could be involved in feeding behavior (63, 64), and Glut-11 is a melanin-concentrating hormone (MCH; gene name, *Pmch*) neuron, which is a sub-population of neurons in the lateral hypothalamus (Fig. 6D–E and Suppl. Fig. S10A). A gene ontology (GO) analysis showed that the top signature genes in each cluster were enriched in the GOs consistent with their known biological functions. For instance, GOs regarding ‘synaptic transmission’ and ‘neurotransmitter’ were specifically enriched in the

neuronal clusters, and GOs regarding ‘immune process’ were specifically enriched in the microglial cluster (Fig. 6F). No significant difference in the number of cells in each cluster was found between the grafted and control groups (Fig. 6G).

Next, we performed a differential gene expression (DEG) analysis on each cluster to examine the cell-specific changes that could be mediating the anti-aging effect of the intra-hypothalamic htNSC-transplantation. Interestingly, no statistically significant DEGs were detected in the pan-GABA and pan-Glut clusters (Fig. 6H). By contrast, abundant DEGs were detected in non-neuronal cell clusters. Among them, the microglia showed the most dramatic gene expression changes following intra-hypothalamic htNSC transplantation, which was followed by tanycytes, astrocytes, OPCs, and oligodendrocytes. These findings are consistent with the previous report that glia-specific genes predict age with greater precision than neuron-specific genes (16, 18, 19).

The microglial DEGs that were downregulated in the grafted hypothalami were enriched in the GOs associated with immune response, specifically ‘IκB kinase/NF-κB signaling’ (Fig. 6I). Indeed, the expression of central microglial NF-κB subunits (*Nfkb1*, *Rel*, *Relb*, and *Ikbkg*) were dramatically downregulated in the htNSC-grafted group (Fig. 7A). This is consistent with the hypothalamic microinflammation theory of aging, which is in turn supported by a recent single-cell transcriptomic result about the aged hypothalamic median eminence (65, 66). Specifically, it has been shown that hypothalamic Iκκb and NF-κB are molecules responsible for aging (8, 67) and that htNSCs dampen NF-κB signaling and hypothalamic micro-inflammation in a paracrine manner (68). The microglial genes upregulated by htNSC transplantation were annotated to GOs related to ‘metabolic process,’ specifically ‘lipid metabolism’ (Fig. 6I). Consistently, it has been reported that dysregulated lipid metabolism and lipid accumulation in microglia represent a dysfunctional and pro-inflammatory state in the aging brain (69). Collectively, these findings suggest that the anti-aging effects observed following intra-hypothalamic htNSC transplantation might be attained by correcting the microglial inflammatory and dysregulated lipid metabolic pathways characteristic of aged brains. We further compared gene expression changes in the microglia of grafted hypothalami (vs. vehicle-injected controls) with those of age-associated

microglial genes recorded in multiple published datasets (15, 65, 70). Single-cell expression levels of the microglial genes downregulated during aging in all the published datasets (calculated using 'AddModuleScore' in the Seurat package) were significantly upregulated in the microglia of grafted hypothalami, compared with the levels in the vehicle-treated control hypothalami (p-value <0.05, statistical method Wilcoxon rank-sum test) (Fig. 6J). Concordantly, microglial genes with age-dependent upregulation in the datasets of Chen (2022) and Ximarekis (2019) were significantly downregulated in the microglia of the grafted hypothalami, together indicating that age-dependent microglial signatures were corrected in aged hypothalami by htNSC transplantation.

The tanycyte cluster had enrichment in GOs related to cell-to-cell and intracellular signaling (Fig. 6I). That finding is consistent with the role of naïve tanycytes as the portal between the hypothalamus and the rest of the body, the place where hormones and metabolic cues are exchanged. The most enriched GO in the tanycytes of the grafted hypothalami was 'positive regulation of hydrolase activity.' It has been demonstrated that after being released from hypothalamic neurons, pro-TRH requires hydrolase-mediated activation in tanycytes (24, 71). Therefore, it is possible that htNSC transplantation also restores the tanycyte-mediated TRH signaling process that usually decreases during aging (72).

We further analyzed the htNSC transplantation–mediated DEGs in 23 neuron subclusters characterized by their unique gene expression signatures (Suppl. Fig. S10A). GABA-4 and GABA-6 were the GABAergic neuron clusters whose gene expressions were most highly modulated by htNSC transplantation, whereas Glut-5, Glut-6, Glut-7, and Glut-8 were the most highly affected among the glutamatergic neuronal clusters (Suppl. Fig. S10B and C). Among those, it is noted that GABA-4 was the *Vipr2*+ neuronal population associated with circadian clock, while GABA-6 was identified as *Lef1*+ neuron whose function is unknown (73). In addition, Glut-7 neuron has been identified as the *Ppp1r17*+ neuron that has been reported to exert the feedback inhibitory function of feeding (74).

Loss of cell-to-cell communication is one of the hallmarks of aging. Using known ligand–receptor interactions, it is possible to infer information flow from one cell type to another. A cell-

to-cell communication analysis using CellChat (75) showed that pericyte VEGF signaling was restored by htNSC transplantation (Fig. 6K). Downregulation of the VEGF signal is a major underlying cause of age-dependent blood brain barrier (BBB) dysfunction (76). MCH is an orexic neurohormone that is mainly secreted by GABAergic neurons in the hypothalamus (77). Consistent with the increased body energy metabolism that we saw in the grafted mice, GABAergic neuronal output of MCH (*Pmch*) and neuronal communication with glial cells were diminished in the grafted hypothalami (Fig. 6L). Additionally, alterations in non-canonical WNT and GDF signal–mediated cell–cell communications were also manifested following htNSC transplantation.

Neuro-inflammation in aged hypothalami corrected by intra-hypothalamic htNSC implantation

Next, we validated the snRNA-seq data indicating that hypothalamic inflammation subsided following htNSC transplantation by examining protein levels with immunofluorescence staining. Consistent with the snRNA-seq data, the abundance of IBA1+ microglia and GFAP+ astrocytes in the hypothalamus were not altered by htNSC transplantation (Suppl. Fig. S11A–B). Additionally, no morphologic differences in microglia or astrocytes were found between groups (Suppl. Fig. S11A–B). However, the number of phosphorylated p65 (activated p65) positive cells was greatly reduced in the transplanted group, as well as its co-expression in microglia and astrocyte (Fig. 7B). It has been shown that glial activation of the NF-κB signal results in systemic metabolic dysregulation, including glucose intolerance and obesity (78). Additionally, a marked reduction in CD68+ cells and a decline in microglial TNF-α expression in the grafted hypothalamus were confirmed both in the snRNA-seq and in immunohistochemical analysis (Fig. 7C–D). Finally, consistent with the snRNA-seq data, we observed significant reduction of caspase-1 and IL1-β immunoreactive cells, signifying inactivation of inflammasome pathway (Fig. 7E–F). Consequently, we observed increased neuronal activity in the transplanted group as evaluated by C-FOS+ cells (Suppl. Fig. S12), implying an improvement in hypothalamic activity in sensing and responding to peripheral metabolic cues (79). Collectively, these findings strongly support that the anti-aging effects observed in the grafted mice were at least in part attained by correcting micro-inflammation and reactive glial phenotypes in their aged hypothalami.

DISCUSSION

In this study we demonstrated that htNSCs derived from hPSCs exhibits health-span promoting benefits when transplanted by ameliorating age-associated dysregulation of body metabolism and physiology. The correction of age-associated changes was accompanied by increased energy metabolism and glucose tolerance, with upregulated browning/thermogenic/catabolic, and sympathetic adrenergic gene and protein expression and reduced expression of senescence proteins (in the kidney), overall suggesting improved energy homeostasis and lipid metabolism. Considering that the hypothalamus is the master coordinator of a myriad of homeostatic functions that are deregulated during aging, the anti-aging effects observed in this study are likely to reflect the central action of the grafted human htNSCs (or their differentiated progenies) in rejuvenating host hypothalamus cells or environment to allow systemic body metabolism to be more efficiently regulated via hypothalamic control of the autonomic nervous system or metabolic hormonal action in systemic circulation. Vice versa, dysregulation of peripheral lipid metabolism causes chronic inflammation of the hypothalamus in models of high-fat diet-fed mice or APOE4/APOE-KO mice (80, 81), which suggests a feed-forward mechanism between the improved systemic body metabolism and hypothalamic inflammation in the transplanted mice.

In addition to changes in their body/energy metabolism and physiology, the mice grafted with human htNSCs in this study and mouse htNSCs in the study of Zhang et al. (8) showed improved memory and cognitive functioning. Several explanations could be given for how cognitive memory is improved by intra-hypothalamic transplantation. First, based on previous studies reporting that cognitive decline is caused by metabolic disturbance (82, 83), the improvement of memory and cognitive functions in the grafted mice could be a consequence of improved systemic body/energy metabolism. An emerging concept posits brain insulin resistance as a relevant condition linking metabolic disorders with cognitive deterioration (82, 84).

(85-87). In addition, it has been shown that the deposition of visceral adipose tissue induces systemic inflammation (88) and impairs memory and cognition in mice via IL1-mediated microglial activation in the hippocampus (89). Thus, considering that peripheral fat deposition was reduced by intra-hypothalamic htNSC transplantation in this study, the blockage of peripheral-brain inflammatory crosstalk is another possible mechanism underlying the improved brain functioning. Second, the hypothalami rejuvenated by htNSC transplantation could directly regulate memory and cognitive activity via hypothalamic-hippocampal neurocircuitry networks (1-3) and para-/endocrine factors secreted by hypothalamic neuronal cells, such as VGF (4), FGF21 (90, 91) and pregnenolone (5).

The aged hypothalamus is characterized by chronic inflammation that impairs its ability to control systemic body metabolism (92), and thus hypothalamic micro-inflammation is thought to underlie systemic aging (66, 93). It has also been shown that hypothalamic inflammation is reduced by anti-aging drugs (94). The single-cell transcriptome and immunohistochemical analyses in this study revealed that neuro-inflammation was substantially corrected in host hypothalami grafted with human htNSCs derived from hPSCs. Consistently, grafted NSCs have been reported to have anti-inflammatory action (95-97). However, a potential therapeutic contribution by the differentiated htNSC progeny cannot be excluded. For example, astrocytes differentiated from the grafted htNSCs might also have an anti-inflammatory function (98-100). In addition, astrocytes and tanycytes derived from the grafted htNSCs could contribute to anti-aging effects by supporting endogenous hypothalamic neuronal functioning (11, 27, 101), sensing peripheral metabolic cues (22, 23), and controlling the hormonal output of the hypothalamic-pituitary-thyroid axis (24).

It has previously been shown that glial cells, not neuronal populations, are mainly affected by age-related changes (16, 18, 19). Consistently, the transcriptome changes in the grafted hypothalami were mainly enriched in the non-neuronal hypothalamic populations: oligodendrocytes, OPCs, astrocytes, tanycytes, and microglia. The expression of genes in the NF-κB, TNF-α, and inflammasome pathways of astrocytes and microglia, as well as the expression of microglial genes that increase during aging (70), were downregulated following

htNSCs implantation, collectively underscoring the appropriateness of targeting glial cells in the hypothalamus when developing anti-aging therapies.

In conclusion, this study has shown that implanting human htNSCs derived from hPSC-organoids holds therapeutic promise for healthy aging or slowing the aging process. However, despite our efforts, the mechanism underlying the anti-aging effects we observed remains elusive, so future research is needed. The human htNSC culture system and mouse model for intra-hypothalamic htNSC transplantation developed in this study could be used in future research to attain a deeper understanding of hypothalamic physiology and support the clinical realization of anti-aging therapy.

MATERIAL AND METHODS

Reagents and resources

Detailed information of reagents and resources used in this paper can be found in Supplemental Table S1.

Cell culture

hESCs (H9) and hiPSCs (CMC-hIPSC-011, CS-001) were cultured on Matrigel-coated plates in feeder-free conditions in mTeSR-1 medium (Stemcell Technologies, Vancouver, Canada). As schematized in Fig. 1A, human htNSCs were prepared by adopting the organoid-based NSC preparation method that was recently published by our group (33). First, to generate human hypothalamus-like organoids , hESCs or hiPSCs were seeded at a density of 5,000 cells/well in a low-attachment, 96-well, round-bottom plate in neural induction medium (N2:Neurobasal, 1:1, Thermo Fisher Scientific, Waltham, Massachusetts) containing 2% B27 without vitamin A (Thermo Fisher Scientific), 200 μM ascorbic acid (MilliporeSigma, Burlington, Massachusetts), and 25 mg/L insulin, (Thermo Fisher Scientific). The ROCK inhibitor Y27632 (20 μM, MilliporeSigma) was added for 24 hours after cell seeding. Hypothalamus patterning of the differentiating hESCs/hiPSCs was induced by adding SB431542 (10 μM, Tocris, Bristol, UK) and noggin (200 ng/ml, Peprotech, Cranbury, New Jersey) for days 0–7 and adding sonic hedgehog (SHH, 100 ng/mL, Peprotech) and purmorphamine (2 μM, MilliporeSigma) for days 1–13. The medium was replenished every other day. Floating spheres (organoids) were transferred into low attachment, 6-well plates (16 spheres/well) on day 13 in neural expansion medium (N2 containing 16 μg/L insulin, 200 μM ascorbic acid, 100 U/ml penicillin G, and 100 μg/ml streptomycin) supplemented with bFGF (20 ng/mL, Peprotech), a mitogen for NSC, and cultured on an orbital shaker (80 rpm) until day 20. The organoids enriched with htNSCs were chopped, dissociated with Acutase (Stemcell Technologies), and plated on poly-L-ornithine/fibronectin-coated plates in bFGF-supplemented neural expansion medium. The htNSCs were expanded with cell passages at 5–7-day intervals. Y27632 was added for only 1 day after each cell passage. Terminal differentiation of the htNSCs was induced in N2 medium supplemented with 200 μM ascorbic acid, 10 ng/mL BDNF (Peprotech), 10 ng/mL GDNF

(Peprotech), 1 μM db-cAMP (MilliporeSigma), and penicillin/streptomycin. As a control, NSCs with ventral midbrain identity (ventral midbrain-type NSCs; VM-NSCs) were prepared as described previously (33).

Animal care and study approval

Middle-aged C57BL/6J male mice (11–12 months) were purchased from the Korean Basic Science Institute (Gwangju, South Korea) or Jackson Laboratory (Yokohama, Japan) and young-aged C57BL/6J male mice (2–3 months) were purchased from Korean Basic Science Institute (Gwangju, South Korea). All mice housed in a specific pathogen-free barrier facility with a temperature of 23 ± 1°C, a humidity of 50 ± 10%, a 12 h light/dark cycle, and free access to food (standard chow, 5053 PicoLab Rodent Diet 20, Lab Diet, Saint Louis, Missouri) and water. All procedures for the animal experiments were approved by the Hanyang College of Medicine Institutional Animal Care and Use Committee (IACUC) (approval number, 2018-0217A and 2020-0142A) and the Korean Institute of Science and Technology (KIST) IACUC and Institutional Biosafety Committee (Approval number, KIST-2019-048).

Transplantation procedures

For cell transplantation, 12-month-old mice received stereotaxic surgery under anesthesia induced by a mixture of Zoletil (37.5 mg/kg) and Rompun (5.83 mg/kg) in isotonic saline. Human htNSC dissociated into single-cells using Accutase and subsequently suspended in 1μl of N2 medium (1×10^5 cells/μL) were injected into the MBH (AP: –1.5 mm, ML: ±0.4 mm, DV: –5.6 mm) at a rate of 0.25 μL/minute for 2 minutes using 26G needle, and the injector was then left in place for an additional 5 minutes before removal. A sham operation with an N2 medium injection was carried out for the control group. The animals received daily injections of cyclosporine A (10 mg/kg, i.p.) starting 1 day before the grafting and continuing for 3 weeks.

Behavioral analyses

All behavioral tests were performed in the behavioral testing room. An ANY-maze video-tracking system (Stoelting, Wood Dale, Illinois) equipped with a digital camera connected to a

computer was used. The following behavior tests were conducted in compliance with the ARRIVE guidelines. Detailed analyses in the Supplemental Methods.

Measurement of systemic body metabolism

Assays for body composition, metabolic cage experiment, glucose tolerance test, body temperature, bone density measurement, and bone histomorphometry are described in the Supplemental Methods.

Histological analysis

Mice were transcardially perfused with 30 mL of PBS (pH 7.4), followed by 30 mL of 4% paraformaldehyde (PFA) in PBS. Their brains were dissected out and post-fixed with 4% PFA overnight at 4°C and then transferred to 30% sucrose for 7 days for cryoprotection. The cryoprotected brains were frozen in TissueTek OCT compound (Sakura Finetek, Torrance, California) and sliced into 30 µm sections using a cryostat (Leica, Nussloch, Germany). For peripheral tissues, the WAT, BAT, livers, and femurs were dissected from the mice without fixation and divided into two halves for histochemical and Western blot analyses. The tissues for histochemical staining were fixed overnight at 4°C in 4% PFA in PBS, paraffin embedded, and sectioned into 4 µm slices that were stained with hematoxylin and eosin (H&E) following the standard procedure.

Determination of protein and mRNA expressions

Protein expressions in the htNSC cultures and mouse hypothalamic tissues were assessed using immunostaining and Western blot analyses. Serum levels of cytokines and leptin were also determined using a Proteome Profiler Mouse XL Cytokine Array and a Mouse/Rat Leptin Quantikine ELISA Kit (R&D Systems, Minneapolis, Minnesota), respectively. mRNA expressions were assessed using quantitative PCR, global, and single cell transcriptomic analyses. Detailed methods are described in the Supplemental Methods.

Statistical analysis

No statistical method was used to predetermine sample sizes, which were chosen with adequate statistical power based on literature and experience. Data shown from representative experiments were repeated with similar results in at least 3 independent experiments, unless otherwise indicated by sample size. Homogeneity of variance was tested using F-test for two groups, and Brown-Forsythe test for more than two groups. Data were analyzed using two-tailed unpaired Student's t-testing, one-way analysis of variance (ANOVA), or Mann-Whitney U-testing. Welch's correction was applied for datasets with unequal variance. Tukey post-hoc test was used for one-way ordinary ANOVA test while unpaired t-testing was used for one-way Welch ANOVA test. All multiple testing p-values were adjusted using Benjamini and Hochberg correction. For behavioral analyses, all data points below or above mean ± 1.645 * SD (corresponding to 5% in the normal distribution) are considered as outliers and were removed from statistical analyses. Additional analyses using linear mixed modeling and Monte-Carlo permutation (n = 10,000) were applied in behavior datasets. In all cases, results were considered statistically significant when $p < 0.05$. Error bars show the mean ± standard error of the mean (SEM) or the median, and p values are represented as: *$p < 0.05$, **$p < 0.01$, ***$p < 0.001$, and ****$p < 0.0001$. Statistical analyses were performed with Prism software version 8 (GraphPad Software) or R.

Data availability

The datasets produced in this study are available in the following databases:

hPSCs-derived htNSC bulk RNA-seq: GSE214877

hPSCs-derived htNSC organoid scRNA-seq: GSE215174

htNSC-transplanted aged mouse hypothalamus snRNA-seq: GSE215174

Values for each data point presented in this paper can be found in the Supporting Data Values XLS file.

Acknowledgements

Fundings: This work was supported by grants 2020M3A9D8039920, KFRM 23A0104L1, 2017R1A5A2015395, 2022R1I1A1A01071091, and 2013M3A9D5072550 funded by the

National Research Foundation of Korea (NRF) of the Ministry of Science and ICT, Republic of Korea, and by the research fund of Corestem Inc., Republic of Korea.

Author contribution: S.H.L. and M.S.K. supervised the project. S.H.L., M.S.K., Y.A.S., Y.L., and K.P. designed experiments, and drafted and revised the manuscript. Y.A.S., Y.L., K.P., S.H., J.K., M.J.S., N-K.L., K-S.P., T.H., S.C., K.W.K., D.J.Y., W-Y.P., K.Y.H., S.G.Y., I.Y.K., and J.K.S. performed experiments. Y.A.S., Y.L., and K.P. analyzed and interpreted data, and performed statistical analyses. S.H.L., M.S.K., Y.A.S., J.K.S., T.Y.L., and M.S.K. acquired funding.

Declaration of interests: S.H.L. and Y.A.S. are inventors on a patent related to the differentiation of neural stem cells from pluripotent stem cells. The remaining authors declare no competing interest.

References

1. Zhou W, He Y, Rehman AU, Kong Y, Hong S, Ding G, et al. Loss of function of NCOR1 and NCOR2 impairs memory through a novel GABAergic hypothalamus-CA3 projection. *Nat Neurosci.* 2019;22(2):205-17.
2. Chen S, He L, Huang AJY, Boehringer R, Robert V, Wintzer ME, et al. A hypothalamic novelty signal modulates hippocampal memory. *Nature.* 2020;586(7828):270-4.
3. Li YD, Luo YJ, Chen ZK, Quintanilla L, Cherasse Y, Zhang L, et al. Hypothalamic modulation of adult hippocampal neurogenesis in mice confers activity-dependent regulation of memory and anxiety-like behavior. *Nat Neurosci.* 2022;25(5):630-45.
4. Beckmann ND, Lin WJ, Wang M, Cohain AT, Charney AW, Wang P, et al. Multiscale causal networks identify VGF as a key regulator of Alzheimer's disease. *Nature communications.* 2020;11(1):3942.
5. Ramirez S, Haddad-Tovolli R, Radosevic M, Toledo M, Pane A, Alcolea D, et al. Hypothalamic pregnenolone mediates recognition memory in the context of metabolic disorders. *Cell metabolism.* 2022;34(2):269-84 e9.
6. Paul A, Chaker Z, and Doetsch F. Hypothalamic regulation of regionally distinct adult neural stem cells and neurogenesis. *Science.* 2017;356(6345):1383-6.
7. Kim K, and Choe HK. Role of hypothalamus in aging and its underlying cellular mechanisms. *Mechanisms of ageing and development.* 2019;177:74-9.
8. Zhang Y, Kim MS, Jia B, Yan J, Zuniga-Hertz JP, Han C, et al. Hypothalamic stem cells control ageing speed partly through exosomal miRNAs. *Nature.* 2017;548(7665):52-7.

9. Garcia-Caceres C, Quarta C, Varela L, Gao Y, Gruber T, Legutko B, et al. Astrocytic Insulin Signaling Couples Brain Glucose Uptake with Nutrient Availability. *Cell.* 2016;166(4):867-80.
10. Chowen JA, Argente-Arizon P, Freire-Regatillo A, Frago LM, Horvath TL, and Argente J. The role of astrocytes in the hypothalamic response and adaptation to metabolic signals. *Progress in neurobiology.* 2016;144:68-87.
11. Garcia-Caceres C, Balland E, Prevot V, Luquet S, Woods SC, Koch M, et al. Role of astrocytes, microglia, and tanycytes in brain control of systemic metabolism. *Nat Neurosci.* 2019;22(1):7-14.
12. Ameroso D, Meng A, Chen S, Felsted J, Dulla CG, and Rios M. Astrocytic BDNF signaling within the ventromedial hypothalamus regulates energy homeostasis. *Nat Metab.* 2022.
13. Clarke LE, Liddelow SA, Chakraborty C, Munch AE, Heiman M, and Barres BA. Normal aging induces A1-like astrocyte reactivity. *Proceedings of the National Academy of Sciences of the United States of America.* 2018;115(8):E1896-E905.
14. Suda Y, Nakashima T, Matsumoto H, Sato D, Nagano S, Mikata H, et al. Normal aging induces PD-1-enriched exhausted microglia and A1-like reactive astrocytes in the hypothalamus. *Biochem Biophys Res Commun.* 2021;541:22-9.
15. Galatro TF, Holtman IR, Lerario AM, Vainchtein ID, Brouwer N, Sola PR, et al. Transcriptomic analysis of purified human cortical microglia reveals age-associated changes. *Nat Neurosci.* 2017;20(8):1162-71.
16. Soreq L, Consortium UKBE, North American Brain Expression C, Rose J, Soreq E, Hardy J, et al. Major Shifts in Glial Regional Identity Are a Transcriptional Hallmark of Human Brain Aging. *Cell reports.* 2017;18(2):557-70.
17. Boisvert MM, Erikson GA, Shokhirev MN, and Allen NJ. The Aging Astrocyte Transcriptome from Multiple Regions of the Mouse Brain. *Cell reports.* 2018;22(1):269-85.
18. Ximerakis M, Lipnick SL, Innes BT, Simmons SK, Adiconis X, Dionne D, et al. Single-cell transcriptomic profiling of the aging mouse brain. *Nat Neurosci.* 2019;22(10):1696-708.
19. Wang W, Wang M, Yang M, Zeng B, Qiu W, Ma Q, et al. Transcriptome dynamics of hippocampal neurogenesis in macaques across the lifespan and aged humans. *Cell research.* 2022;32(8):729-43.
20. Li J, Tang Y, and Cai D. IKKbeta/NF-kappaB disrupts adult hypothalamic neural stem cells to mediate a neurodegenerative mechanism of dietary obesity and pre-diabetes. *Nature cell biology.* 2012;14(10):999-1012.
21. Lee DA, Bedont JL, Pak T, Wang H, Song J, Miranda-Angulo A, et al. Tanycytes of the hypothalamic median eminence form a diet-responsive neurogenic niche. *Nat Neurosci.* 2012;15(5):700-2.
22. Balland E, Dam J, Langlet F, Caron E, Steculorum S, Messina A, et al. Hypothalamic tanycytes are an ERK-gated conduit for leptin into the brain. *Cell metabolism.* 2014;19(2):293-301.
23. Langlet F. Tanycytes: a gateway to the metabolic hypothalamus. *J Neuroendocrinol.* 2014;26(11):753-60.

24. Muller-Fielitz H, Stahr M, Bernau M, Richter M, Abele S, Krajka V, et al. Tanycytes control the hormonal output of the hypothalamic-pituitary-thyroid axis. *Nature communications.* 2017;8(1):484.
25. Pierce AA, and Xu AW. De novo neurogenesis in adult hypothalamus as a compensatory mechanism to regulate energy balance. *The Journal of neuroscience.* 2010;30(2):723-30.
26. Kokoeva MV, Yin H, and Flier JS. Neurogenesis in the hypothalamus of adult mice: potential role in energy balance. *Science.* 2005;310(5748):679-83.
27. Bolborea M, Pollatzek E, Benford H, Sotelo-Hitschfeld T, and Dale N. Hypothalamic tanycytes generate acute hyperphagia through activation of the arcuate neuronal network. *Proceedings of the National Academy of Sciences of the United States of America.* 2020;117(25):14473-81.
28. Wang L, Meece K, Williams DJ, Lo KA, Zimmer M, Heinrich G, et al. Differentiation of hypothalamic-like neurons from human pluripotent stem cells. *The Journal of clinical investigation.* 2015;125(2):796-808.
29. Merkle FT, Maroof A, Wataya T, Sasai Y, Studer L, Eggan K, et al. Generation of neuropeptidergic hypothalamic neurons from human pluripotent stem cells. *Development.* 2015;142(4):633-43.
30. Ogawa K, Suga H, Ozone C, Sakakibara M, Yamada T, Kano M, et al. Vasopressin-secreting neurons derived from human embryonic stem cells through specific induction of dorsal hypothalamic progenitors. *Scientific reports.* 2018;8(1):3615.
31. Qian X, Jacob F, Song MM, Nguyen HN, Song H, and Ming GL. Generation of human brain region-specific organoids using a miniaturized spinning bioreactor. *Nature protocols.* 2018;13(3):565-80.
32. Song B, Cha Y, Ko S, Jeon J, Lee N, Seo H, et al. Human Autologous iPSC-Derived Dopaminergic Progenitors Restore Motor Function in Parkinson's Disease Models. *The Journal of clinical investigation.* 2019.
33. Kim SW, Woo HJ, Kim EH, Kim HS, Suh HN, Kim SH, et al. Neural stem cells derived from human midbrain organoids as a stable source for treating Parkinson's disease: Midbrain organoid-NSCs (Og-NSC) as a stable source for PD treatment. *Progress in neurobiology.* 2021;204:102086.
34. Xiao YZ, Yang M, Xiao Y, Guo Q, Huang Y, Li CJ, et al. Reducing Hypothalamic Stem Cell Senescence Protects against Aging-Associated Physiological Decline. *Cell metabolism.* 2020;31(3):534-48 e5.
35. Artegiani B, Lyubimova A, Muraro M, van Es JH, van Oudenaarden A, and Clevers H. A Single-Cell RNA Sequencing Study Reveals Cellular and Molecular Dynamics of the Hippocampal Neurogenic Niche. *Cell reports.* 2017;21(11):3271-84.
36. Hochgerner H, Zeisel A, Lonnerberg P, and Linnarsson S. Conserved properties of dentate gyrus neurogenesis across postnatal development revealed by single-cell RNA sequencing. *Nat Neurosci.* 2018;21(2):290-9.
37. Zeisel A, Hochgerner H, Lonnerberg P, Johnsson A, Memic F, van der Zwan J, et al. Molecular Architecture of the Mouse Nervous System. *Cell.* 2018;174(4):999-1014 e22.
38. Fleck JS, Sanchis-Calleja F, He Z, Santel M, Boyle MJ, Camp JG, et al. Resolving organoid brain region identities by mapping single-cell genomic data to reference atlases. *Cell Stem Cell.* 2021;28(6):1148-59 e8.

39. Herb BR, Glover HJ, Bhaduri A, Colantuoni C, Bale TL, Siletti K, et al. Single-cell genomics reveals region-specific developmental trajectories underlying neuronal diversity in the human hypothalamus. *bioRxiv.* 2022:2021.07.20.453090.
40. Quinn JP, Kandigian SE, Trombetta BA, Arnold SE, and Carlyle BC. VGF as a biomarker and therapeutic target in neurodegenerative and psychiatric diseases. *Brain Commun.* 2021;3(4):fcab261.
41. Lewis JE, Brameld JM, and Jethwa PH. Neuroendocrine Role for VGF. *Front Endocrinol (Lausanne).* 2015;6:3.
42. Herrero-Navarro A, Puche-Aroca L, Moreno-Juan V, Sempere-Ferrandez A, Espinosa A, Susin R, et al. Astrocytes and neurons share region-specific transcriptional signatures that confer regional identity to neuronal reprogramming. *Sci Adv.* 2021;7(15).
43. Hochstim C, Deneen B, Lukaszewicz A, Zhou Q, and Anderson DJ. Identification of positionally distinct astrocyte subtypes whose identities are specified by a homeodomain code. *Cell.* 2008;133(3):510-22.
44. Wang H, Ke Z, Alimov A, Xu M, Frank JA, Fang S, et al. Spatiotemporal expression of MANF in the developing rat brain. *PLoS One.* 2014;9(2):e90433.
45. Yang S, Yang H, Chang R, Yin P, Yang Y, Yang W, et al. MANF regulates hypothalamic control of food intake and body weight. *Nature communications.* 2017;8(1):579.
46. Lepko T, Pusch M, Muller T, Schulte D, Ehses J, Kiebler M, et al. Choroid plexus-derived miR-204 regulates the number of quiescent neural stem cells in the adult brain. *EMBO J.* 2019;38(17):e100481.
47. Hasel P, Rose IVL, Sadick JS, Kim RD, and Liddelow SA. Neuroinflammatory astrocyte subtypes in the mouse brain. *Nat Neurosci.* 2021;24(10):1475-87.
48. Mizrak D, Levitin HM, Delgado AC, Crotet V, Yuan J, Chaker Z, et al. Single-Cell Analysis of Regional Differences in Adult V-SVZ Neural Stem Cell Lineages. *Cell reports.* 2019;26(2):394-406 e5.
49. Romanov RA, Tretiakov EO, Kastriti ME, Zupancic M, Haring M, Korchynska S, et al. Molecular design of hypothalamus development. *Nature.* 2020;582(7811):246-52.
50. Gupta D, and Morley JE. Hypothalamic-pituitary-adrenal (HPA) axis and aging. *Compr Physiol.* 2014;4(4):1495-510.
51. Cuevas-Ramos D, Mehta R, and Aguilar-Salinas CA. Fibroblast Growth Factor 21 and Browning of White Adipose Tissue. *Front Physiol.* 2019;10:37.
52. Flippo KH, and Potthoff MJ. Metabolic Messengers: FGF21. *Nat Metab.* 2021;3(3):309-17.
53. Mullican SE, and Rangwala SM. Uniting GDF15 and GFRAL: Therapeutic Opportunities in Obesity and Beyond. *Trends Endocrinol Metab.* 2018;29(8):560-70.
54. Tsai VWW, Husaini Y, Sainsbury A, Brown DA, and Breit SN. The MIC-1/GDF15-GFRAL Pathway in Energy Homeostasis: Implications for Obesity, Cachexia, and Other Associated Diseases. *Cell metabolism.* 2018;28(3):353-68.
55. Masand R, Paulo E, Wu D, Wang Y, Swaney DL, Jimenez-Morales D, et al. Proteome Imbalance of Mitochondrial Electron Transport Chain in Brown Adipocytes Leads to Metabolic Benefits. *Cell metabolism.* 2018;27(3):616-29 e4.

56. Vernochet C, Mourier A, Bezy O, Macotela Y, Boucher J, Rardin MJ, et al. Adipose-specific deletion of TFAM increases mitochondrial oxidation and protects mice against obesity and insulin resistance. *Cell metabolism.* 2012;16(6):765-76.
57. Tran LT, Park S, Kim SK, Lee JS, Kim KW, and Kwon O. Hypothalamic control of energy expenditure and thermogenesis. *Exp Mol Med.* 2022;54(4):358-69.
58. Sharan K, and Yadav VK. Hypothalamic control of bone metabolism. *Best Pract Res Clin Endocrinol Metab.* 2014;28(5):713-23.
59. Omori S, Wang TW, Johmura Y, Kanai T, Nakano Y, Kido T, et al. Generation of a p16 Reporter Mouse and Its Use to Characterize and Target p16(high) Cells In Vivo. *Cell metabolism.* 2020;32(5):814-28 e6.
60. Ostlund RE, Jr., Yang JW, Klein S, and Gingerich R. Relation between plasma leptin concentration and body fat, gender, diet, age, and metabolic covariates. *J Clin Endocrinol Metab.* 1996;81(11):3909-13.
61. Minocci A, Savia G, Lucantoni R, Berselli ME, Tagliaferri M, Calo G, et al. Leptin plasma concentrations are dependent on body fat distribution in obese patients. *Int J Obes Relat Metab Disord.* 2000;24(9):1139-44.
62. Elefteriou F, Takeda S, Ebihara K, Magre J, Patano N, Kim CA, et al. Serum leptin level is a regulator of bone mass. *Proceedings of the National Academy of Sciences of the United States of America.* 2004;101(9):3258-63.
63. Idelevich A, Sato K, Nagano K, Rowe G, Gori F, and Baron R. Neuronal hypothalamic regulation of body metabolism and bone density is galanin dependent. *The Journal of clinical investigation.* 2018;128(6):2626-41.
64. Qualls-Creekmore E, Yu S, Francois M, Hoang J, Huesing C, Bruce-Keller A, et al. Galanin-Expressing GABA Neurons in the Lateral Hypothalamus Modulate Food Reward and Noncompulsive Locomotion. *The Journal of neuroscience.* 2017;37(25):6053-65.
65. Chen ZH, Li S, Xu M, Liu CC, Ye H, Wang B, et al. Single-cell transcriptomic profiling of the hypothalamic median eminence during aging. *J Genet Genomics.* 2022;49(6):523-36.
66. Cai D, and Khor S. "Hypothalamic Microinflammation" Paradigm in Aging and Metabolic Diseases. *Cell metabolism.* 2019;30(1):19-35.
67. Zhang G, Li J, Purkayastha S, Tang Y, Zhang H, Yin Y, et al. Hypothalamic programming of systemic ageing involving IKK-beta, NF-kappaB and GnRH. *Nature.* 2013;497(7448):211-6.
68. Liu Y, Guo YF, Peng H, Zhou HY, Su T, Yang M, et al. Hypothalamic Hnscr regulates glucose balance by mediating central inflammation and insulin signal. *Cell Prolif.* 2022:e13332.
69. Marschallinger J, Iram T, Zardeneta M, Lee SE, Lehallier B, Haney MS, et al. Lipid-droplet-accumulating microglia represent a dysfunctional and proinflammatory state in the aging brain. *Nat Neurosci.* 2020;23(2):194-208.
70. Lopes KP, Snijders GJL, Humphrey J, Allan A, Sneeboer MAM, Navarro E, et al. Genetic analysis of the human microglial transcriptome across brain regions, aging and disease pathologies. *Nature genetics.* 2022;54(1):4-17.

71. Rodriguez-Rodriguez A, Lazcano I, Sanchez-Jaramillo E, Uribe RM, Jaimes-Hoy L, Joseph-Bravo P, et al. Tanycytes and the Control of Thyrotropin-Releasing Hormone Flux Into Portal Capillaries. *Front Endocrinol (Lausanne).* 2019;10:401.
72. Daimon CM, Chirdon P, Maudsley S, and Martin B. The role of Thyrotropin Releasing Hormone in aging and neurodegenerative diseases. *Am J Alzheimers Dis (Columbia).* 2013;1(1).
73. Chiba A, and Honma Y. Distribution of neuropeptide Y-like immunoreactivity in the brain and hypophysis of the cloudy dogfish, Scyliorhinus torazame. *Cell Tissue Res.* 1992;268(3):453-61.
74. Caglar C, and Friedman J. Restriction of food intake by PPP1R17-expressing neurons in the DMH. *Proceedings of the National Academy of Sciences of the United States of America.* 2021;118(13).
75. Jin S, Guerrero-Juarez CF, Zhang L, Chang I, Ramos R, Kuan CH, et al. Inference and analysis of cell-cell communication using CellChat. *Nature communications.* 2021;12(1):1088.
76. Wen SW, and Wong CHY. Aging- and vascular-related pathologies. *Microcirculation.* 2019;26(2):e12463.
77. Jego S, Glasgow SD, Herrera CG, Ekstrand M, Reed SJ, Boyce R, et al. Optogenetic identification of a rapid eye movement sleep modulatory circuit in the hypothalamus. *Nat Neurosci.* 2013;16(11):1637-43.
78. Zhang Y, Reichel JM, Han C, Zuniga-Hertz JP, and Cai D. Astrocytic Process Plasticity and IKKbeta/NF-kappaB in Central Control of Blood Glucose, Blood Pressure, and Body Weight. *Cell metabolism.* 2017;25(5):1091-102 e4.
79. Kovacs LA, Furedi N, Ujvari B, Golgol A, and Gaszner B. Age-Dependent FOSB/DeltaFOSB Response to Acute and Chronic Stress in the Extended Amygdala, Hypothalamic Paraventricular, Habenular, Centrally-Projecting Edinger-Westphal, and Dorsal Raphe Nuclei in Male Rats. *Front Aging Neurosci.* 2022;14:862098.
80. Dutheil S, Ota KT, Wohleb ES, Rasmussen K, and Duman RS. High-fat diet induced anxiety and anhedonia: impact on brain homeostasis and inflammation. *Neuropsychopharmacology.* 2016;41(7):1874-87.
81. Wang X, Yang J, Lu T, Zhan Z, Wei W, Lyu X, et al. The effect of swimming exercise and diet on the hypothalamic inflammation of ApoE-/-mice based on SIRT1-NF-κB-GnRH expression. *Aging (Albany NY).* 2020;12(11):11085.
82. Biessels GJ, and Despa F. Cognitive decline and dementia in diabetes mellitus: mechanisms and clinical implications. *Nat Rev Endocrinol.* 2018;14(10):591-604.
83. Tanaka H, Gourley DD, Dekhtyar M, and Haley AP. Cognition, Brain Structure, and Brain Function in Individuals with Obesity and Related Disorders. *Curr Obes Rep.* 2020;9(4):544-9.
84. Sripetchwandee J, Chattipakorn N, and Chattipakorn SC. Links Between Obesity-Induced Brain Insulin Resistance, Brain Mitochondrial Dysfunction, and Dementia. *Front Endocrinol (Lausanne).* 2018;9:496.
85. Wirth M, Lange C, Huijbers W, and Alzheimer's Disease Neuroimaging I. Plasma cortisol is associated with cerebral hypometabolism across the Alzheimer's disease spectrum. *Neurobiol Aging.* 2019;84:80-9.

86. Marbouti L, Zahmatkesh M, Riahi E, and Shafiee Sabet M. GnRH protective effects against amyloid beta-induced cognitive decline: A potential role of the 17beta-estradiol. *Mol Cell Endocrinol.* 2020;518:110985.
87. Xiong J, Kang SS, Wang Z, Liu X, Kuo TC, Korkmaz F, et al. FSH blockade improves cognition in mice with Alzheimer's disease. *Nature.* 2022;603(7901):470-6.
88. Osborn O, and Olefsky JM. The cellular and signaling networks linking the immune system and metabolism in disease. *Nat Med.* 2012;18(3):363-74.
89. Guo DH, Yamamoto M, Hernandez CM, Khodadadi H, Baban B, and Stranahan AM. Visceral adipose NLRP3 impairs cognition in obesity via IL-1R1 on CX3CR1+ cells. *The Journal of clinical investigation.* 2020;130(4):1961-76.
90. Timper K, Del Rio-Martin A, Cremer AL, Bremser S, Alber J, Giavalisco P, et al. GLP-1 Receptor Signaling in Astrocytes Regulates Fatty Acid Oxidation, Mitochondrial Integrity, and Function. *Cell metabolism.* 2020;31(6):1189-205 e13.
91. Taliyan R, Kakoty V, Kc S, and Kumari S. Fibroblast Growth Factor 21 and Autophagy Modulation Ameliorates Amyloid beta-Induced Alzheimer Disease Pathology in Rats. *Alzheimers Dement.* 2021;17 Suppl 2:e058695.
92. Jais A, and Bruning JC. Hypothalamic inflammation in obesity and metabolic disease. *The Journal of clinical investigation.* 2017;127(1):24-32.
93. Bhusal A, Rahman MH, and Suk K. Hypothalamic inflammation in metabolic disorders and aging. *Cellular and molecular life sciences : CMLS.* 2021.
94. Sadagurski M, Cady G, and Miller RA. Anti-aging drugs reduce hypothalamic inflammation in a sex-specific manner. *Aging Cell.* 2017;16(4):652-60.
95. Peruzzotti-Jametti L, Bernstock JD, Vicario N, Costa ASH, Kwok CK, Leonardi T, et al. Macrophage-Derived Extracellular Succinate Licenses Neural Stem Cells to Suppress Chronic Neuroinflammation. *Cell Stem Cell.* 2018;22(3):355-68 e13.
96. Pluchino S, Zanotti L, Rossi B, Brambilla E, Ottoboni L, Salani G, et al. Neurosphere-derived multipotent precursors promote neuroprotection by an immunomodulatory mechanism. *Nature.* 2005;436(7048):266-71.
97. Pluchino S, Gritti A, Blezer E, Amadio S, Brambilla E, Borsellino G, et al. Human neural stem cells ameliorate autoimmune encephalomyelitis in non-human primates. *Annals of neurology.* 2009;66(3):343-54.
98. Wang J, Jiang P, Deng W, Sun Y, and Liu Y. Grafted human ESC-derived astroglia repair spinal cord injury via activation of host anti-inflammatory microglia in the lesion area. *Theranostics.* 2022;12(9):4288-309.
99. Song JJ, Oh SM, Kwon OC, Wulansari N, Lee HS, Chang MY, et al. Cografting astrocytes improves cell therapeutic outcomes in a Parkinson's disease model. *The Journal of clinical investigation.* 2018;128(1):463-82.
100. Yang Y, Song JJ, Choi YR, Kim SH, Seok MJ, Wulansari N, et al. Therapeutic functions of astrocytes to treat alpha-synuclein pathology in Parkinson's disease. *Proceedings of the National Academy of Sciences of the United States of America.* 2022;119(29):e2110746119.
101. Prevot V, and Sharif A. The polygamous GnRH neuron: Astrocytic and tanycytic communication with a neuroendocrine neuronal population. *J Neuroendocrinol.* 2022:e13104.

Figure

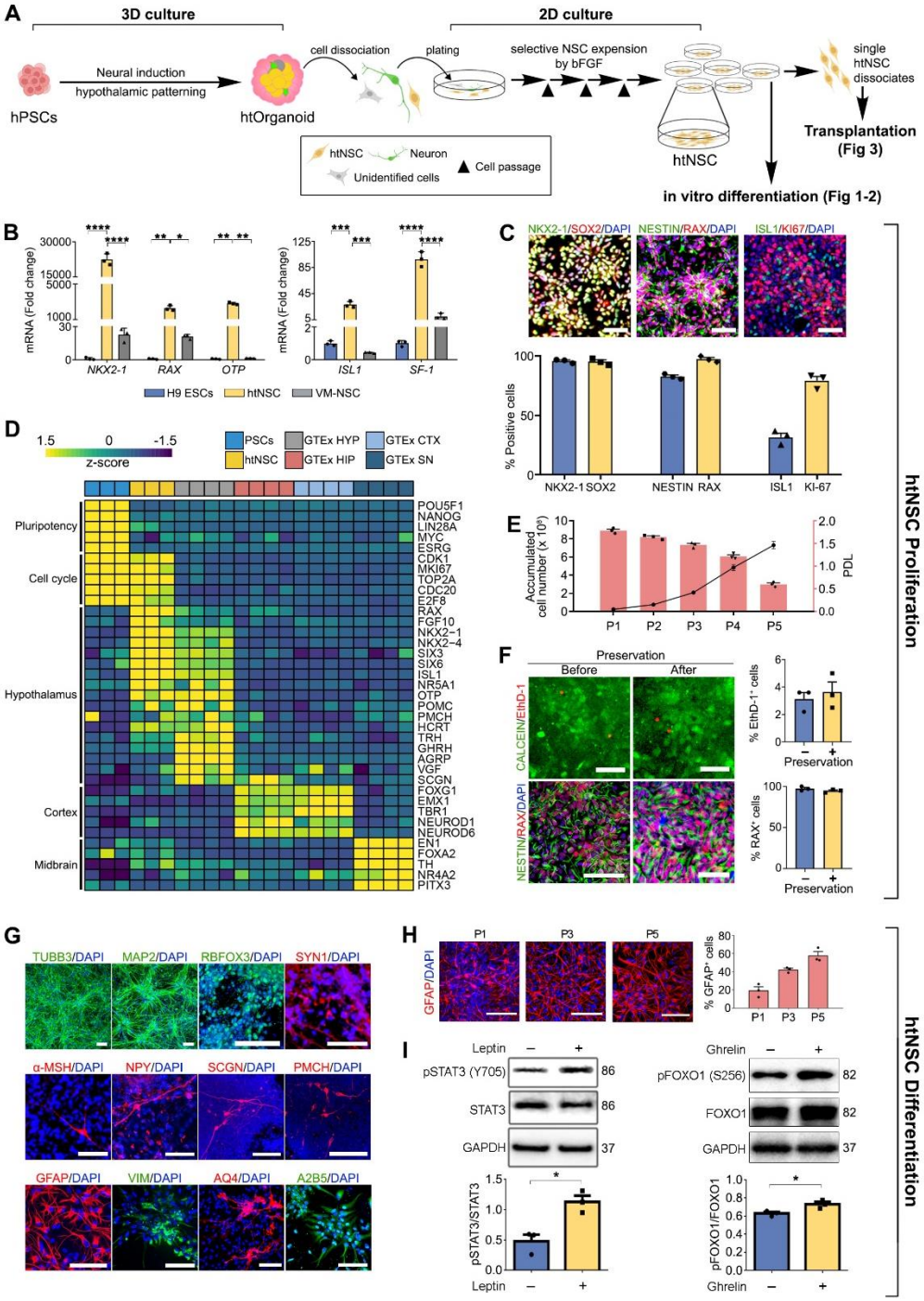

Fig. 1. Derivation of hypothalamic neural stem cells (htNSCs) from hPSC-derived hypothalamus-like organoids.

A. An overview of the protocol to yield htNSCs with proliferative and neuro-/gliogenic potential from hPSC-derived organoid cultures.

B. mRNA expression of htNSC-specific marker genes (*NKX2-1*, *RAX*, *OTP*, *ISL1*, *SF1*) assessed by qRT-PCR. The expression levels in the H9 hESC-derived htNSCs were compared with those in undifferentiated hESCs and hESC-derived ventral midbrain-type neural stem cells (VM-NSCs). n=3.[a,b]

C. Immunocytochemical detection of generic NSC (SOX2, NESTIN, KI67) and htNSC-specific markers (NKX2-1, RAX, ISL1). Scale bars, 100 µm. n=3.[a]

D. Heatmap comparison of our H9 hESC-derived htNSC transcriptome with various human adult brain regions in the GTEx database. HYP: hypothalamus; HIP: hippocampus; CTX: cortex; SN: substantia nigra.

E. Cell expansion, estimated using a cell growth curve (line) and the population doubling level (PDL, bar). PDL=log(N/No)/log2, where N is the number of cells at the end of each passage, and No is the number of cells initially plated. n=3.[a]

F. Storage of htNSCs in liquid N2 without altering cell viability (Calcein/EthD-1) or htNSC-specific marker expression (NESTIN/RAX). Scale bars, 100 µm. n=3.[a,b]

G. Terminal differentiation of htNSCs to yield hypothalamus-specific neuronal and astroglial progeny. The cellular identities were evaluated on htNSC differentiation day 40 by the expression of general neuronal (TUBB3, MAP2, RBFOX3, SYN1), hypothalamus neuron subtype (α-MSH, NPY, SCGN, PMCH), and astroglial (GFAP, VIM, AQ4, A2B5) markers. Scale bars, 100 µm.

H. Cell passage–dependent change in the htNSC differentiation propensity. The astrogenic differentiation potential of the htNSCs gradually increase during the cell passages. Scale bars, 100 µm. n=3.[a]

I. Cells differentiated from htNSCs acquired the hypothalamus-specific functions of responding to leptin and ghrelin ligands. Intracellular STAT3 and FOXO1 activation were evaluated in the differentiated htNSC cultures before and after exogenous leptin and ghrelin treatments, respectively. n=3.[a,b]

[a]Data shown are means ± SEM.

[b]*$p < 0.05$; **$p < 0.01$; ***$p < 0.001$; ****$p < 0.0001$ by two-tailed Student's t testing.

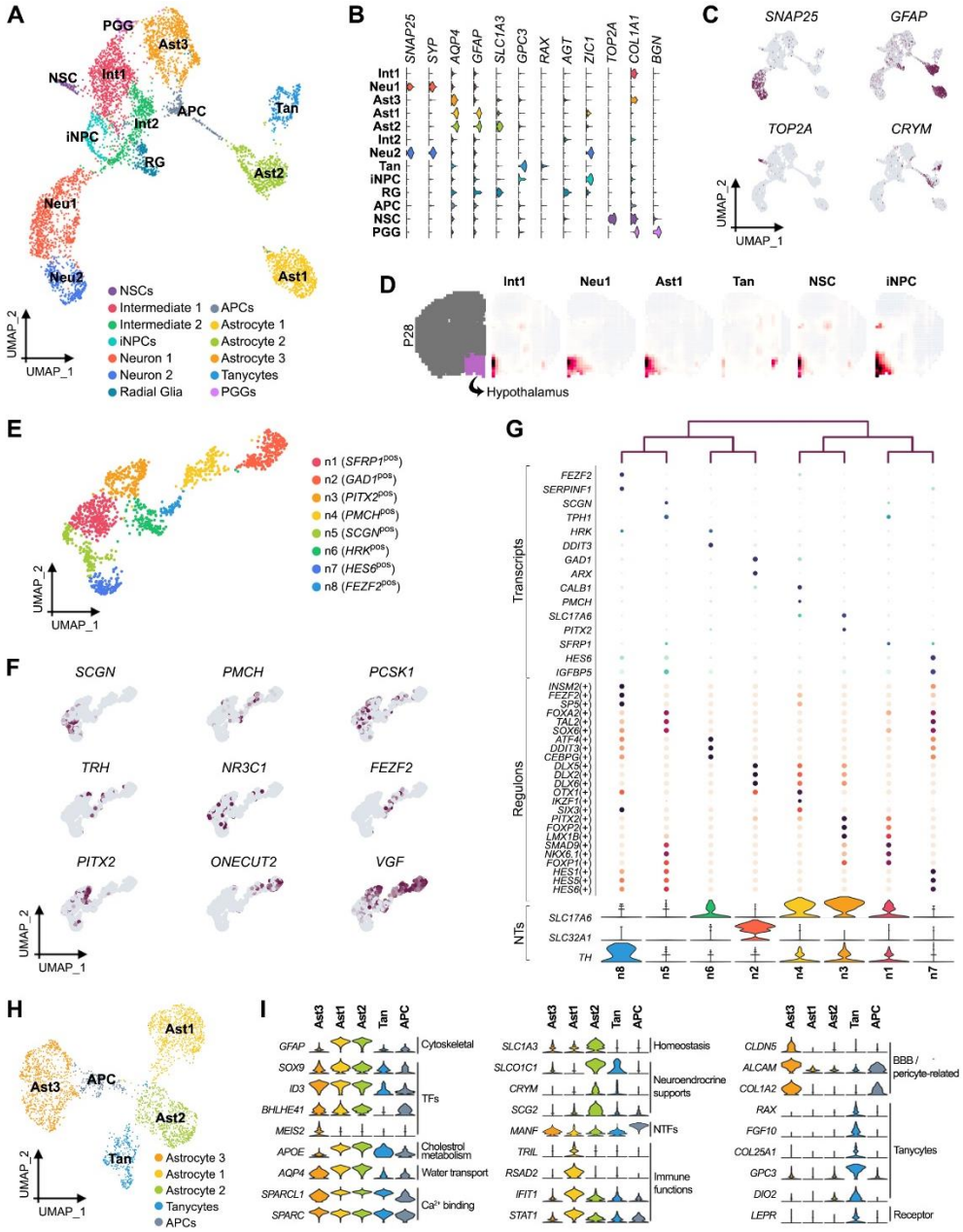

Fig. 2. Single-cell RNA-seq–based identification of cell progeny differentiated from hPSC-derived human htNSC cultures

A. Uniform manifold approximation and projection (UMAP) plot of 6,394 single cells projected into 13 cell clusters (indicated by color). NSCs, neural stem/progenitor cells; Int1, intermediate progenitor cells 1, Int2, intermediate progenitor cells 2; iNPCs, interneuron progenitor cells; APCs, astrocyte progenitor cells; Neu1, neurons 1; Neu2, neurons 2; Ast1, astrocytes 1; Ast2, astrocytes 2; Ast3, astrocytes 3; RG, radial glia; PGG, proteoglycan-secreting glia; Tan, tanycytes.

B–C. Violin (B) and feature (C) plots of representative cell-specific genes from the differentiated cell clusters.

D. Hypothalamic brain identity of the cell clusters validated by voxel-based spatial brain mapping onto the mouse brain at postnatal day 28 (from the Allen Brain Institute).

E. Re-clustering of the neuronal population into 8 subclusters of neurons.

F. Feature plot of representative hypothalamic neuropeptides (*SCGN, PMCH, PNOC, TRH, NR3C1, VGF*) and transcription factors (*FEZF2, PITX2, ONECUT2*).

G. Dot plots of selected transcripts (top) and regulons (middle) with violin plots of neurotransmitter phenotype gene expression (*SLC17A6*, *SLC32A1*, *TH*) (below) in each cluster of the neuronal subtypes.

H–I. UMAP plots of the astrocyte clusters (APC, Ast1, Ast2, Ast3, Tan) with the representative genes whose expression was enriched in each cluster.

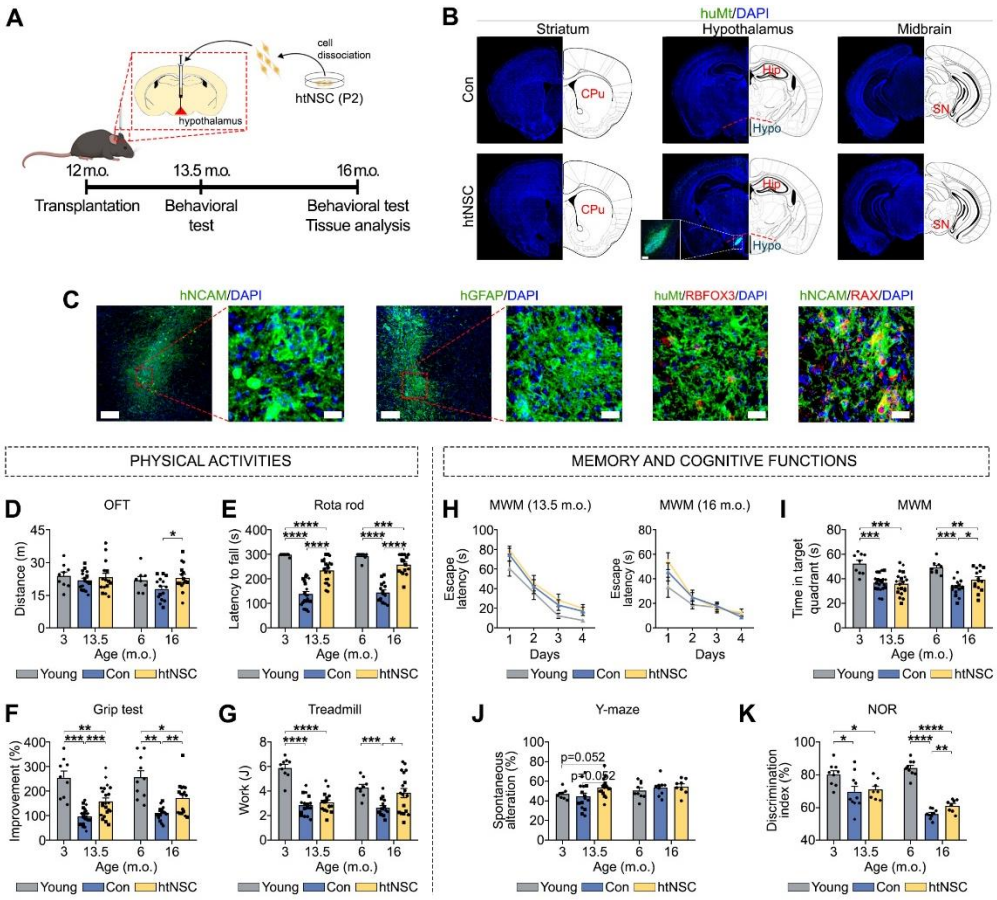

Fig. 3. Age-associated decline in physical and cognitive activities is rescued by intra-hypothalamic htNSC transplantation.

A. Experimental scheme for the animal study. hESC-derived htNSCs (P2) were dissociated into single cells and transplanted into the medio-basal hypothalami of 12-month-old male mice. Behavioral tests were performed 1.5 months and/or 4 months post-transplantation, and tissue analyses were conducted 4 months post-surgery. Four rounds of transplantation experiments were conducted using mice and donor human htNSCs that were independently prepared.

B. Overview images depict the human htNSC-derived graft localized in the mouse hypothalamus but not in other brain regions. The htNSC-derived graft was identified using a human mitochondria-specific antibody (huMt). CPu, caudate putamen; Hip, hippocampus; Hypo, hypothalamus; SN, substansia nigra.

C. Identification of cell types derived from the grafted htNSCs using antibodies specific for human-species (hNCAM, huMt), human-specific astrocytes (hGFAP), htNSCs (RAX), or neurons (RBFOX3) at 2–4 weeks post-transplantation. Scale bars, 50 µm or 200 µm.

D–G. Physical activity, muscle coordination, strength, and endurance were estimated using the open filed test (OFT, C), rotarod (D), grip (E), and treadmill performance (F) tests. n= 9-10 (young), 15-22 (control), 15-22 (transplanted).[a,b]

H–K. Memory and cognitive functions were evaluated using the Morris water maze (MWM, G,H), Y-maze (I), and novel object recognition (NOR, J) tests 4 months post-surgery. n= 9 (young), 9-20 (control), 8-20 (transplanted).[a,b]

[a]Data shown are means ± SEM. The data presented in D-K represent the combined data from at least two independent datasets.

[b]*$p < 0.05$; **$p < 0.01$; ****$p < 0.0001$ by one-way Welch analysis of variance.

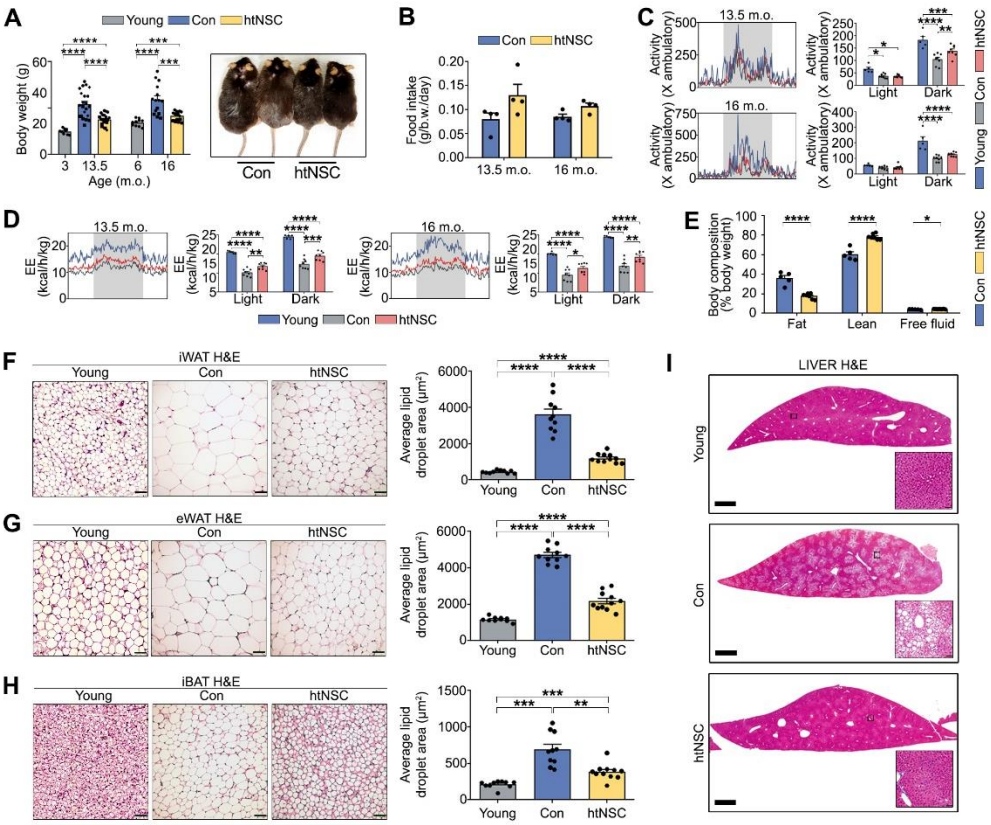

Fig. 4. Intra-hypothalamic human htNSC transplantation improved body energy metabolism and tissue aging in aged mice.

A. The body weights of the control (vehicle-injected) and transplanted mice 1.5 months and 4 months post-transplantation (left) and representative photographs of the mice at 16 months old (right). n= 10 (young), 15 (control), 17 (transplanted).[a,b]

B. Daily food intake (normal chow diet) of the control and transplanted mice. n= 5 (control), 7 (transplanted).[a,b]

C. Measurement of x-ambulatory activity during the light and dark phases of the day at 1.5 months post-transplantation. n= 5 (young), 8 (control), 8 (transplanted).[a,b]

D. Energy expenditure measured in metabolic cages. n= 5 (young), 8 (control), 8 (transplanted).[a,b]

E. NMR-based measurement of the fat and lean masses and free fluid volumes in the vehicle-treated control (n= 5) and transplanted (n = 7) mice.[a,b]

F–H. Quantified lipid droplet areas (right) with representative H&E-stained tissue section images (left) of the iWAT (F), eWAT (G), and iBAT (H) liver from the young (n = 10), control (n= 10) and transplanted (n = 11) mice. Scale bars, 50 μm. [a,b]

I. Representative H&E-stained images of liver from the young (n = 10), control (n= 10) and transplanted (n = 11) mice. Scale bars, 1 mm.

[a]Data shown are means ± SEM. The data presented in A, C-D, and F-I represent the combined data from at least two independent datasets.

[b]*$p < 0.05$; **$p < 0.01$; ****$p < 0.0001$ by one-way analysis of variance or two-tailed Student's t testing.

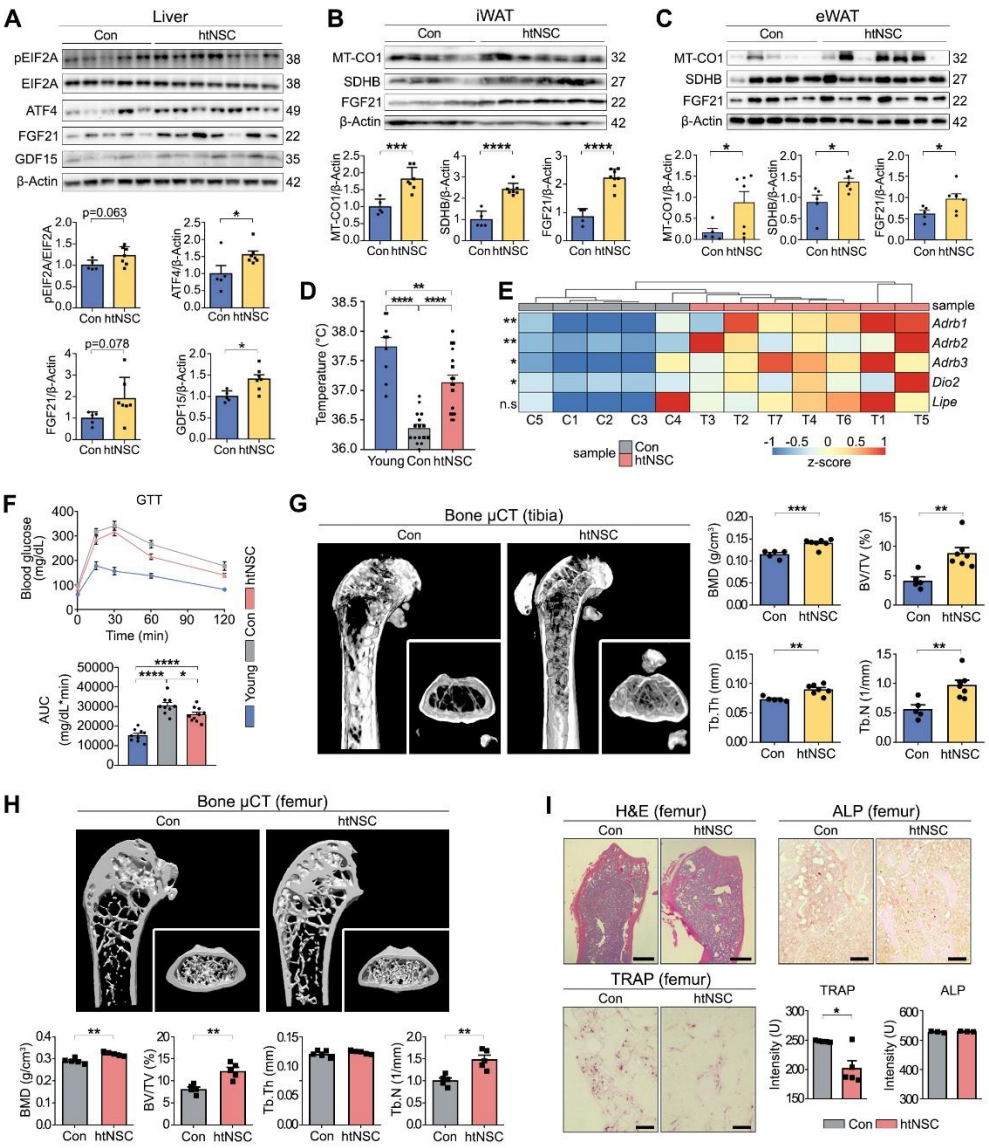

Fig. 5. Body energy and bone metabolism changes ameliorated in aged mice that received htNSC grafts.

A–C. Immunoblot-based quantification of the key regulator proteins for energy metabolism and thermogenesis (browning) in the liver (A), iWAT (B), and eWAT (C) of the control (n=5) and transplanted (n=7) mice. [a,b]

D. Rectal temperature. n = 10 (young), 16 (control), 17 (transplanted).[a,b]

E. qPCR-based quantification of gene expression for β1, 2, and 3 adrenoreceptors *(Adrb1*, *Adrb2*, and *Adrb3*), and lipolytic genes (Dio2 and Lipe). n= 5 (control), 7 (transplanted).[a,b]

F. Glucose tolerance test. Data represent blood glucose levels over the time points after glucose injection (2 g/kg, i.p.) (left) and the integral of the glucose levels during the post-injection period (right). n= 9 (young), 10 (control), 10 (transplanted).[a,b]

G. Representative μCT bone images of tibia (left) and the indices of BMD, BV/TV, Tb.Th., and Tb.N. (right), which increased significantly in the transplanted mice. n= 5 (control), 7 (transplanted).[a,b]

H. Representative μCT bone images of femur (top) and the indices of BMD, BV/TV, Tb.Th., and Tb.N. (below), which increased significantly in the transplanted mice. n= 5.[a,b]

I. Representative bone histomorphometry (H&E, Tartrate-resistant acid phosphatase (TRAP), and Alkaline phosphatase (ALP) staining) images of the femurs with quantification of relative intensity of TRAP-positive osteoclasts and ALP-positive osteoblasts. n= 5 for TRAP staining, 3 for ALP staining. Scale bar, 800 μm (H&E staining) or 100 μm (TRAP and ALP staining). [a,b]

[a]Data shown are means ± SEM. The data presented in D and F represent the combined data from at least two independent datasets.

[b]*$p < 0.05$; **$p < 0.01$; ***$p < 0.001$; ****$p < 0.0001$ by one-way analysis of variance or two-tailed Student's t testing.

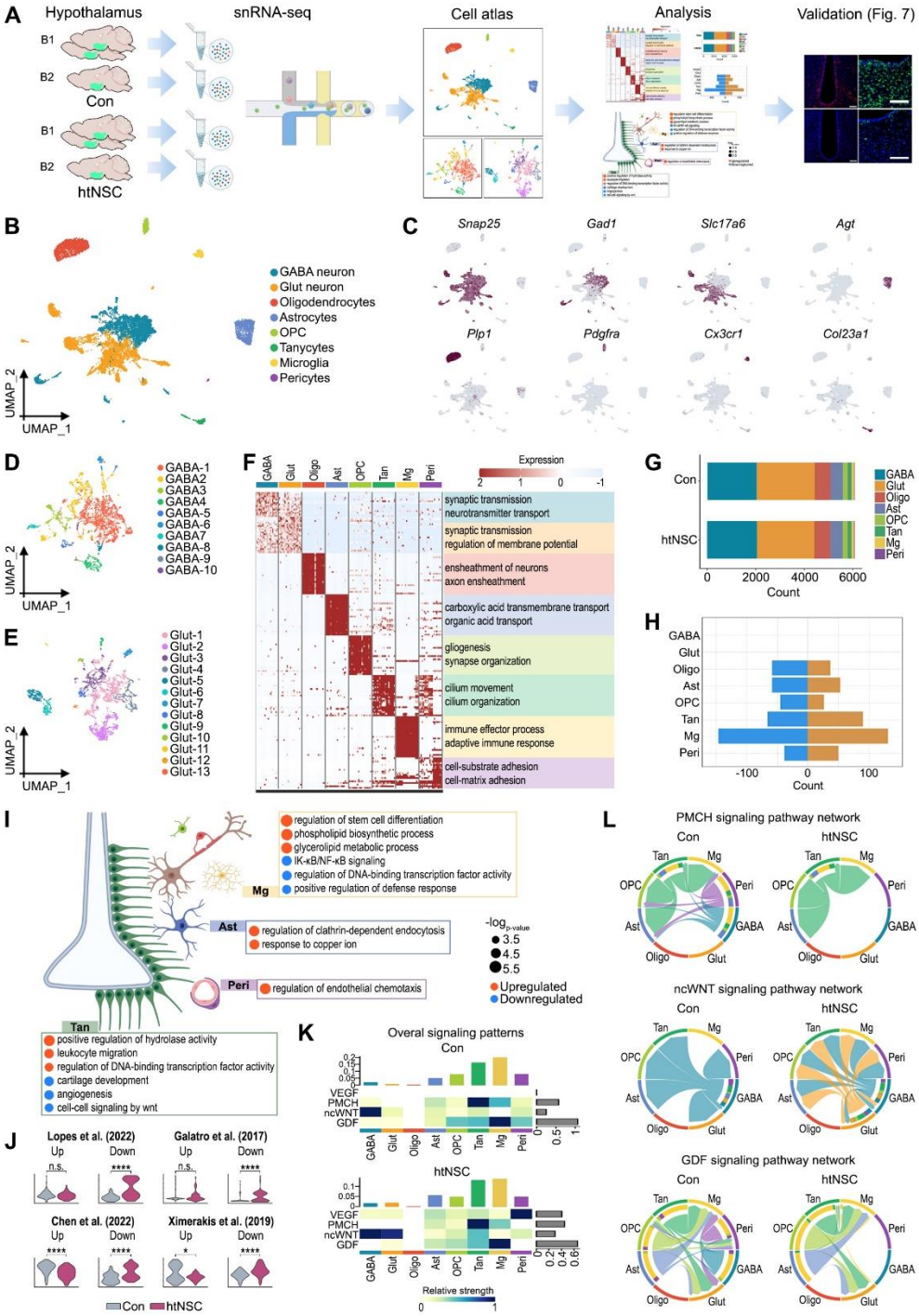

Fig. 6. Single nucleus RNA-seq analysis of transplanted and control hypothalami.

A. Schematic of the snRNA-seq experiment.

B–C. UMAP plot of 12,161 nuclei filtered and processed from control and transplanted hypothalami (B) and feature plot showing representative cluster transcripts (C).

D–E. UMAP plots of the GABA-neuron subcluster (D) and Glut-neuron subcluster (E).

F. Heatmap showing the top 25 signature genes among the clusters and the two most representative GO results.

G. Stacked bar plot showing the composition of each cell type in the dataset for each group.

H. Bar plot showing the number of upregulated (orange) and downregulated (blue) transcripts in all cell types for the transplanted group.

I. GO (biological process) enrichment analysis of DEGs from the non-neuronal clusters.

J. Violin plot of module scores for microglial nuclei in gene sets obtained from various studies. The statistical analysis used the Mann-Whitney test.

K. Subset of a heatmap of the cell-to-cell interaction network showing the overall (ingoing and outgoing) signal strength of VEGF, PMCH, ncWNT, and GDF signaling.

L. Circle plots of an inferred signaling network of PMCH, ncWNT, and GDF signaling.

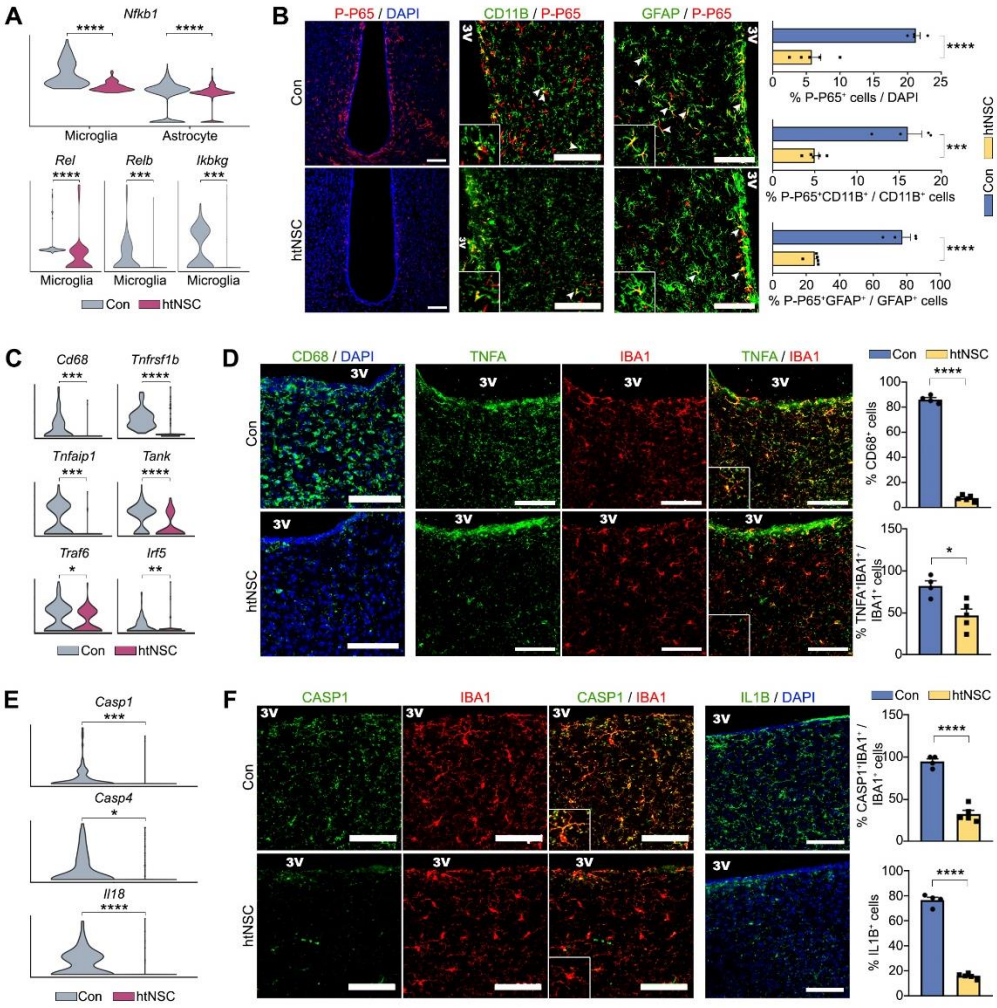

Fig. 7. Neuro-inflammation in aged hypothalami subsided following htNSC transplantation.

A–B. NF-κB signal activation in the aged control and grafted hypothalami, as assessed by snRNA-seq (A) and immunohistochemical (B) analyses. Violin plot of *Nfkb1* in microglial and astrocyte clusters and *Rel*, *Relb*, and *Ikbkg* in microglia from the snRNA-seq data (A). The percentage of p-P65+ in the total (DAPI+), microglial (IBA1+), and astrocytic (GFAP+) cell populations (B). Scale bars, 100 µm. n = 3 (control), 3 (transplanted) in (A)[c,d] and n = 4 (control), 5 (transplanted) in (B)[a,b].

C–D. Hypothalamic inflammation, as estimated by the snRNA-seq analysis of inflammatory gene expression (*Cd68*, *Tnfrsf1b*, *Tnfaip1*, *Tank*, *Traf6*, and *Irf5*) in the microglial clusters (C) and the immunohistochemical analysis for the percentage of CD68+/DAPI+ and TNFA+/IBA1+

cells (D). Scale bars, 100 µm. n = 3 (control), 3 (transplanted) in (C)[c,d] and n = 4 (control), 5 (transplanted) in (D)[a,b].

E–F. SnRNA-seq- and immunohistochemistry-based determination of NLRP3-inflammasome activation in the aged control and grafted hypothalami. Scale bars, 100 µm. n = 3 (control), 3 (transplanted) in (E)[c,d] and n = 4 (control), 5 (transplanted) in (F)[a,b].

[a]Data shown are means ± SEM.

[b]*$p < 0.05$; ***$p < 0.001$; ****$p < 0.0001$ by two-tailed Student's t testing.

[c]Data shown are medians.

[d]*$p < 0.05$; **$p < 0.01$; ***$p < 0.001$; ****$p < 0.0001$ by Mann-Whitney U testing.